Addendum to the COMPASS-II Proposal

The COMPASS Collaboration

v1.4 1.10.2017 19:17

contact: O. Denisov/Torino, J. M. Friedrich/TUM
COMPASS spokespersons
Oleg.Denisov@cern.ch, Jan.Friedrich@cern.ch

The COMPASS Collaboration

Joined Czech group, Prague, Czech Republic
K. Augsten, M. Bodlak, M. Finger, M. Finger jr., M. Jandek, V. Jary, K. Juraskova, A. Kveton,
J. Matousek, A. Nikolovova, J. Novy, M. Pesek, M. Peskova, M. Slunecka, A. Srnka, M. Sulc, J. Tomsa,
M. Virius

CEA-Saclay, IRFU, Gif-sur-Yvette, France
Y. Bedfer, A. Ferrero, N. d'Hose, F. Kunne, D. Neyret, S. Platchkov, A. Vidon

Ruhr-Universität Bochum, Bochum, Germany
W. Meyer, G. Reicherz

Rheinische Friedrich-Wilhems-Universität, Bonn, Germany
M. Ball, J. Barth, R. Beck, D. Eversheim, E. Fotina, R. Joosten, B. Ketzer, F. Klein, M. Mikhasenko,
J. Pretz, R. Reyes Ramos, H. Schmieden, A. Thiel, M. Wagner

Universität Freiburg, Freiburg, Germany
M. Büchele, H. Fischer, M. Gorzellik F. Herrmann, P. Jörg

Universität Mainz, Mainz, Germany
J. Giarra, D. von Harrach, E. M. Kabuß, W. Nowak, M. Ostrick, N. Pierre, J. Pochodzalla, M. B. Veit,
M. Wilfert

Technische Universität München, Munich, Germany
S. Chung, C. Dreisbach, W. Dünnweber, M. A. Faessler, J. M. Friedrich, S. Gerassimov, B. Grube,
S. Huber, F. Kaspar, I. Konorov, F. Krinner, S. Paul, D. Ryabchikov, J. Seyfried, D. Steffen, S. Uhl,
S. Wallner

Matrivani Institute of Experimental Research & Education, Calcutta, India
S. Dasgupta, L. Dhara, A. Roy, S. Sarkara, L. Sinha

Tel Aviv University, Tel Aviv, Israel
J. Lichtenstadt,

INFN, Sezione di Torino, e Università di Torino, Turin, Italy
M. G. Alexeev, A. Amoroso, F. Balestra, M. Chiosso, O. Denisov, I. Gnesi, A. Grasso, A. Ivanov,
A. M. Kotzinian, R. Longo, A. Maggiora, D. Panzieri,B. Parsamyan, F. Tosello

INFN, Sezione di Trieste, e Università di Trieste, Trieste, Italy
J. Agarwala, F. Bradamante, A. Bressan, C. Chatterjee, A. Cicuttin, P. Ciliberti, M. Crespo,
S. Dalla Torre, S. Dasgupta, G. Hamar, A. Kerbizi, S. Levorato, N. Makke, A. Martin, G. Menon,
A. Moretti, L. B. Rizzuto, G. Sbrizzai, A. Szabelski, S. Tessaro, F. Tessarotto

Japanese Group, Yamagata, Japan
N. Doshita, N. Horikawa, S. Ishimoto, T. Iwata, K. Kondo Horikawa, T. Matsuda, Y. Miyachi,
G. Nukazuka, H. Suzuki

National Centre for Nuclear Research and University of Warsaw, Warsaw, Poland
W. Augustyniak, B. Badełek, K. Kurek, B. Marianski, A. Sandacz, P. Sznajder,

Warsaw University of Technology, Warsaw, Poland
R. P. Kurjata, J. Marzec, A.Rychter, K. Zaremba, M. Ziembicki

University of Aveiro, Aveiro, Portugal
C. Azevedo, F. Pereira, J. Veloso

Laboratory of Instrumentation and Experimental Particles Physics, Lisbon, Portugal
P. Bordalo, C. Franco, C. Menezes Pires A. S. Nunes, C. Quintans, S. Ramos, L. Silva, M. Stolarski

JINR, Dubna, Russia

R. Akhunzyanov, G. D. Alexeev, N. V. Anfimov, V. A. Anosov, A. Efremov, V. Frolov,
O. P. Gavrichtchouk, A. Gridin, R. Gushterski, A. Guskov, Yu. Ivanshin, A. Janata, Yu. Kisselev,
O. Kouznetsov, G. V. Meshcheryakov, E. Mitrofanov, N. Mitrofanov, A. Nagaytsev, A. Olshevski,
D. V. Peshekhonov, A. Rybnikov, A. Samartsev, I. A. Savin, A. Selyunin, J. Smolik, P. Zavada,
E. Zemlyanichkina, N. Zhuravlev

P. N. Lebedev Physical Institute of the Russian Academy of Sciences, Moscow, Russia

V. Tskhay, M. Zavertyaev

IHEP, Protvino, Russia

S. V. Donskov, G. V. Khaustov, Yu. A. Khokhlov, V. N. Kolosov, V. F. Konstantinov,
Yu. V. Mikhailov, V. A. Polyakov, V. D. Samoilenko

Polytechnic University, Tomsk, Russia

V. E. Burtsev, A. G. Chumakov, G. Chursin, R. R. Dusaev, I. I. Kuznetsov, E. A. Levchenko,
V. E. Lyubovitskij, S. A. Mamon, K. Sharko, B. Vasilishin

CERN, Genève, Switzerland

G. K. Mallot, O. Subrt, A.Vauth

Academia Sinica, Taipei, Taiwan

W. Chang, C. Hsieh, Y. Lian, M. Quaresma

University of Illinois, Urbana-Champaign, USA

V. Andrieux, F. Gautheron, M. Grosse Perdekamp, R. Heitz, J. H. Koivuniemi, Y. Kulinich,
A. Magnon, N. Makins, M. Meyer, J. Peng, C. K. Riedl

Contents

Executive summary

As outlined in the proposal for the ongoing COMPASS-II programme, the research fields of hadron spectroscopy and hadron structure are closely connected since their very beginnings, leading to the establishment of Quantum Chromodynamics (QCD) of quarks and gluons as the theory of strong interactions. It explains the observed weakening of the interquark forces at short distances or large momentum transfers. QCD not only describes hard processes through perturbative expansions, but also the non-perturbative dynamics of the strong interaction, down to soft and extremely soft processes which are involved in meson spectroscopy and linked to chiral perturbation theory. Also the finite extension of the hadrons, as encoded in the nucleon form factors, is connected to their inner dynamics and thus a decisive test field for QCD.

The COMPASS-II proposal covers three important processes in that context, namely deeply-virtual Compton scattering, Drell-Yan dimuon production off a polarised target, and Primakoff reactions on nuclei giving access to soft pion-photon reactions. This programme is foreseen to be completed in the end of the year 2018, after the second year of data taking for polarised Drell-Yan processes, before the long shutdown period LS2 in 2019 and 2020.

The impressive scientific output of COMPASS and COMPASS-II and the rapid progress in the fields of our investigation make us consider various future scenarios where we could again make important contributions, further exploiting the capabilities of the M2 beam line and of an upgraded spectrometer. They are currently being collected in a Letter of Intent that is planned to be submitted end of this year. It will contain, beyond the usage of the conventional, by now available beams, longer-term perspectives with radiofrequency-separated (kaon) beams, with a physics programme of about 10 years, and is worked out within the CERN Physics Beyond Colliders initiative.

Since the CERN Research Board has approved in the memorandum DG-Dr-RCS-2017-093 an early post-LS2 fixed-target programme and running, the COMPASS-II collaboration has decided to propose two physics cases of the future programme, as an addendum to the ongoing programme for data taking immediately after LS2.

The first program, semi-inclusive DIS on transversely polarized deuterons, is the "missing piece" in the COMPASS data sets on transverse target spin orientations. In 2010, a dedicated run was taken on a transversely polarised proton (NH3) target, which provided pioneering and unique information on transversity and Sivers functions, underlining the importance of transverse spin in the QCD structure of the nucleon and the correctness of conjectures put forward 25 years ago. On the contrary we provided only a marginal (albeit unique) data set for the isoscalar deuteron target. Since the older data have been taken only with the low-aperture SMC target magnet, the statistics can be enhanced by up to a factor 20 within one additional year of data taking, which is proposed here, allowing accurate flavour separation for the new functions.

The second program, elastic muon-proton scattering, represents a new physics case for COMPASS. It was recognized recently that in the context of the currently debated "proton radius puzzle", high-energy muon-proton elastic scattering is a decisive experimental method that is complementary, in part even superior to the manifold of other proposed or ongoing experiments. With a dedicated hydrogen gas target to be contributed by a group in Gatchina, who has developed a similar target for an experiment with electron beams at Mainz, COMPASS-II is seen to be the ideal – in fact the only – place to realize this experiment with multi-GeV muon beams. This very appealing per-

spective includes the incorporation of some new equipment, and also necessitates new developments regarding the readout of the detectors, such that some testing will be indispensable.

In view of these preliminaries, the following running schedule is proposed:

2021: one year of data taking with transverse deuteron target, and at an early stage test measurements for the proton radius measurement

2022: one year of data taking for the proton radius measurement (under the condition of a successful testing phase in 2021)

– PHYSICS CASE –

1 Measurement of semi-inclusive deep inelastic scattering off transversely polarised deuterons

1.1 Introduction

In collinear QCD, when the transverse momentum of the partons is neglected, three parton distribution functions (PDFs) fully describe the nucleon at the twist-two level: the momentum distributions $f_1^q(x)$, the helicity distributions $g_1^q(x)$ and the transversity distributions [1] $h_1^q(x)$, where x is the Bjorken variable. On the other hand, a sizable transverse momentum of quarks was derived from the measured azimuthal asymmetries of hadrons produced in unpolarised semi-inclusive deep inelastic scattering (SIDIS) and of the lepton pairs produced in Drell-Yan (DY) processes. Taking into account a finite intrinsic transverse momentum k_T, in total eight transverse momentum dependent (TMD) distribution functions are required to fully describe the nucleon at leading twist [2, 3, 4]. Presently, PDFs that describe non-perturbative properties of hadrons are not yet calculable in QCD from first principles, but their first moments can already be computed in lattice QCD. In the SIDIS cross-section they appear convoluted with fragmentation functions (FFs) [5, 6], so that they can be extracted from the data.

Since transverse spin couples naturally to intrinsic transverse momentum, the resulting correlations are encoded in various TMD PDFs and TMD FFs. Particularly interesting is therefore the measurement of the SIDIS cross-section when the target nucleon is transversely polarized. In this case 8 (5 in case of unpolarised lepton beam) different spin-dependent azimuthal modulations are expected, from which invaluable information on the TMD PDFs can be extracted [1]. In this domain the HERMES and the COMPASS collaborations have performed pioneering measurements and shown beyond any possible doubt the correctness of three most interesting recent conjectures:

- The Sivers function: in a nucleon that is polarized transversely to its momentum the quark distribution is not left-right symmetric with respect to the plane defined by the directions of the nucleon spin and momentum. This asymmetry of the distribution function is called the Sivers effect, and the asymmetric distribution is known as the Sivers distribution function [8].

- The Transversity function: the quarks in a transversely polarized nucleon are transversely polarized. Their polarization is described by the h_1 PDFs which a priori are different and have different properties from the helicity PDFs.

- The Collins function: the hadronization of a transversely polarized quark is not left-right symmetric with respect to the plane defined by the quark momentum and the quark spin [9]. This fact has been exploited to measure the quark transverse polarization in a transversely polarized nucleon, namely the quark transversity PDF.

HERMES [10] and COMPASS [11, 12, 13] are up to now the only SIDIS experiments that have shown that the Sivers function, the Transversity function and the Collins function are different from zero. Independent evidence that the Collins effect is non zero has been provided at the e^+e^- colliders, by looking at the azimuthal correlations of hadrons produced in opposite jets [14, 15], so that global analyses using the SIDIS and the e^+e^- data could result in the extraction of the quark transversity PDF [16, 17].

---

[1] For a review of the notation we refer to the Appendix A of the memo CERN-SPSC-2009-025 SPSC-M-769, SPSLC-P-297 Add.2 [7], which for completeness is also added to this document as section 1.6.

The non zero results for the Collins and the Sivers asymmetries were obtained on proton targets. COMPASS has also measured transverse spin asymmetries using a deuteron target [18]. The accuracy of the data is definitely inferior to that of the proton data, and all the results were compatible with zero, hinting at a possible cancellation between u and d quarks. More recently data have been collected at much lower energy at JLab on a ^{3}He target, essentially a transversely polarized neutron target: the measured asymmetries [19, 20] are also compatible with zero, but the error bars are fairly large. The COMPASS data are still today the only SIDIS data ever taken on a transversely polarised deuteron target, they are necessary to flavor separate the PDFs, and provide constraints on the d-quark contribution.

We propose to perform a one-year measurement scattering the M2 muon beam at 160 GeV/c momentum on a transversely polarized deuteron target, so that, combining the new deuteron data with the good precision proton data collected in the year 2010, the u- and d-distribution functions can be extracted from the SIDIS asymmetry data with comparable accuracies. Due to the late delivery of the COMPASS polarized target magnet, this precise measurement could not be carried through in the early years of data taking when the low statistics sample was collected. Also, the knowledge gained in the last few years (thanks also to the COMPASS results) has by now made the physics case very clear and strong, and we regard this measurement as necessary to complete the exploratory COMPASS programme on transverse spin.

1.2 The case for muon scattering on transversely polarized deuterons

High energy muon scattering on transversely polarized deuterons will provide in a standard 150 days run a wealth of data and complement the data sample collected in 2010 on transversely polarized protons. In the previous section the case for the transversity and the Sivers PDFs was singled out since these effects represent novel and unexpected features, and because there is still hope that these two phenomena could explain the very large transverse spin asymmetries observed since more than 40 years in hadron-hadron scattering. From the present data several extractions of the transversity and of the Sivers PDFs have been performed. As an example Fig. 1 shows the results of the point-by-point extractions of the transversity and the Sivers PDFs using all the existing COMPASS p and d data [21, 22] compared to the extractions done using also the HERMES data [23, 24]. It is immediately apparent that the accuracy of the d-quark PDFs is considerably inferior to that of the u-quark and this is the straightforward motivation for this proposal.

The case for the Collins asymmetry will be detailed in the next section. Here we will summarize the other measurements which will be performed in parallel using the new deuteron data.

In the SIDIS regime the data will allow the extraction of

- **the Sivers function**. As underlined in Ref. [22], and clear from fig. 1, the d_v Sivers function is poorly determined from the present data, and even its sign is not unambiguously fixed by the measurements. The new data will allow to improve on its accuracy by the same factor as for the transversity PDF, namely by a factor 2 to 4 as explained in the next sections.

- **Sivers function of the gluon**. On the theoretical side, the interest on the Sivers function of the gluon is steadily growing. An analysis of all the COMPASS data has provided some indication that the gluon Sivers function might be different from zero [25], but the accuracy of the existing deuteron data is worse by a factor
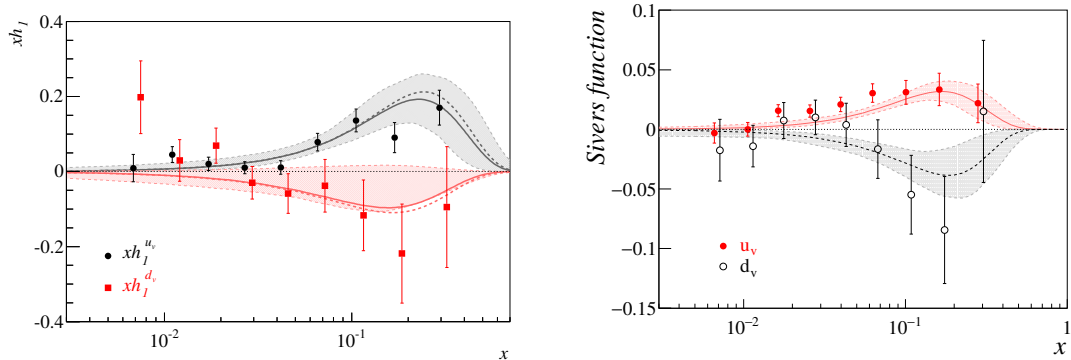
Figure 1: The transversity and the Sivers PDFs extracted point-by-point using the existing COMPASS p and d data from Ref. [21, 22]. The curves are the results of fits to the COMPASS and HERMES data. Note that the uncertainty band for the d-quark transversity would be larger if the Soffer bound was not imposed.

of about 2 than that of the proton data, and also for this specific case new data would be helpful.

In a related analysis the Sivers asymmetry of the J/Ψ has also been determined, since in some models it is related to the gluon Sivers asymmetry [26]. That analysis can also be repeated and considerably improved with the new deuteron data.

- **two hadron asymmetries**. he transverse polarization of a fragmenting quark can also be assessed from the azimuthal modulation of the plane containing two oppositely charged hadrons of the jet. This di-hadron asymmetry can be expressed as the product of the quark transversity distribution and a chiral-odd di-hadron FF, H_1^q, which survives after integration over the two hadron momenta, and thus can be analyzed in the framework of collinear factorization. The high energy of the beam and the large acceptance of the COMPASS spectrometer have allowed us to collect in 2010 a large sample of (oppositely charged) hadron pairs. From the measured di-hadron asymmetries and from corresponding Belle data fairly precise estimates of the u-quark transversity distribution could be obtained [21, 27], while the d-quark extraction has considerably larger uncertainties, very much as for the Collins asymmetry case. Also, a unique and original comparison [13, 28] between the single-hadron Collins asymmetry and the di-hadron asymmetry could be performed. The conclusion of this investigation was that both the single hadron and the di-hadron transverse-spin dependent fragmentation functions are driven by the same elementary mechanism, which is very well described in the $^3P_0$ recursive string fragmentation model [29, 30]. A corresponding analysis with the deuteron data was not possible because of the small statistics of the two hadron data sample due to the use of the SMC small acceptance PT magnet in the first three years of COMPASS running with the deuteron target. The new deuteron data therefore will provide more information both on the transversity PDFs and on the di-hadron FF.

- **the g_2 structure function**. In the naive parton model g_2 is expected to be zero, thus its measurement provides information on the quark-gluon interaction. In COMPASS we have started an analysis to extract g_2 from the 2010 proton data, which will be repeated with the new deuteron data.

Moreover, COMPASS has performed the first ever multidimensional extraction of the whole set of target transverse spin dependent azimuthal asymmetries using the proton data collected in 2010 [31]. Various multi-differential configurations have been tested exploring the $x - Q^2 - z - p_T$ phase-space. Very interesting correlations have been noticed in particular for the Sivers function, This analysis was not possible with the existing deuteron data, but will be done with the new data.

Recently COMPASS has extracted p_T weighted Sivers asymmetries from the 2010 proton data. Also in this case only new accurate data will allow the same analysis to be performed on the deuteron target.

Finally, precise results on deuteron will be produced for all the other SIDIS Transversal Spin Asymmetries (TSA).

In exclusive vector meson production COMPASS has produced several interesting results. In a first paper [32] we published the transverse target spin azimuthal asymmetry $A_{UT}^{\sin(\phi-\phi_S)}$ in hard exclusive production of ρ^0 mesons which we measured both on transversely polarized protons and deuterons. The measured asymmetry is sensitive to the nucleon helicity-flip generalized parton distributions E_q, which are related to the orbital angular momentum of quarks in the nucleon. A second publication [33] used the high statistics proton data collected in 2010, and presented results for all 8 possible transverse target spin asymmetries. In particular a specific combination of two of these asymmetries indicates a signal from the so called "transversity GPD" (i.e. GPD with the helicity flip of exchanged quark). Concerning deuterons, only the results on the $A_{UT}^{\sin(\phi-\phi_S)}$ asymmetry are published [32], due to the poor statistics of the existing deuteron COMPASS data. Very much as for the SIDIS case, however, a combined analysis of both proton and deuteron data is necessary to disentangle the u and d quark GPDs, thus new accurate deuteron data are essential to carry through this analysis. In parallel, the exclusive production of ω will also be measured. The cross-section is smaller by about a factor 10 than for ρ^0 mesons and the detection of the two photons further reduces the ω event sample with respect to the ρ^0, but a combined analysis of ρ^0 and ω mesons provide strong constrains in disentangling the u and d quark contributions.

1.3 The case for transversity

In this section the case for the Collins asymmetry and the extraction of transversity for the u and d quarks will be detailed. The measurement of the quark transversity distributions, which are defined in terms of the nucleon matrix element of the quark tensor current, is particularly important because it provides access to the quark tensor charges δq, which are given by the integral

$$\delta q(Q^2) = \int_0^1 dx [h_1^q(x, Q^2) - h_1^{\bar{q}}(x, Q^2)] \tag{1}$$

In a non-relativistic quark model, h_1^q is equal to g_1^q, and δq is equal to the valence quark contribution to the nucleon spin. The difference between h_1^q and g_1^q provides important constraints to any model of the nucleon. Knowing the quark tensor charges one can construct the isovector nucleon tensor charge $g_T = \delta u - \delta d$, a fundamental property of the nucleon which, together with the vector and axial charge, characterizes the nucleon as a whole. Since many years the tensor charge is being calculated with steadily increasing accuracy by lattice QCD [34]. More recently, its connection with possible novel tensor interactions at the TeV scale in neutron and nuclear β-decays and its possible contribution
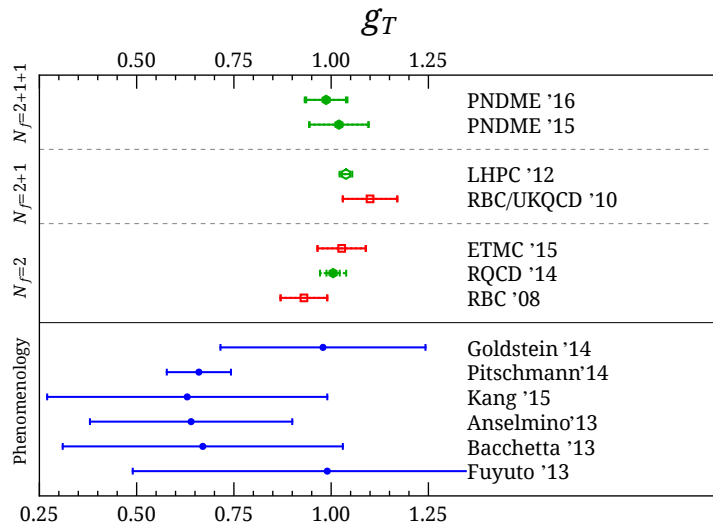
Figure 2: A summary plot showing the current estimates of g_T^{u-d} from Ref. [35].

to the neutron EDM have also been investigated [35], and possible constraints on new physics beyond the standard mode have also been derived [36].

The present knowledge on g_T is well summarized in Fig. 2, from Ref. [35]. The huge difference between the accuracy of the extractions from the existing data and from the QCD lattice simulations is striking and more experimental data are needed. In the near future the only planned and approved experiments will run at JLab12 [37, 38], with very good statistics but $x > 0.05$ and relatively small Q^2.

We propose to measure during one full year, as soon as the LS2 will be over, SIDIS on a transversely polarized deuteron target in the M2 muon beam line. The polarized target system will be reassembled at the end of the DVCS/SIDIS run, this fall, to be used for the Drell-Yan run of 2018, and will stay installed in Hall 888 for this new measurement. The main objective of the measurement is to improve considerably the accuracy of the extraction of h_1^d, but the precision of h_1^u will also improve, by a factor 1.5-2 in the valence region $(x > 0.1)$, as will be shown in the next section.

The COMPASS data will provide large Q^2 data in the x-range covered by JLab, which is very important to evaluate the size of the Q^2 evolution, and will provide lower-x data (down to $x = 0.003$) which are essential both to perform the integrals necessary to evaluate the tensor charges and to estimate the transversity of the sea quarks. The phase space covered by the different experiments is shown in Fig. 3. Clearly the experiment we propose is unique and complementary to the JLab12 experiments.

In the longer term the planned Electron Ion Collider (EIC) has the potential to carry on a very good program scattering at high $\sqrt{s}$ electrons on transversely polarized protons, but its start is not yet well defined in time, and colliding polarized deuterons is not in the core program.
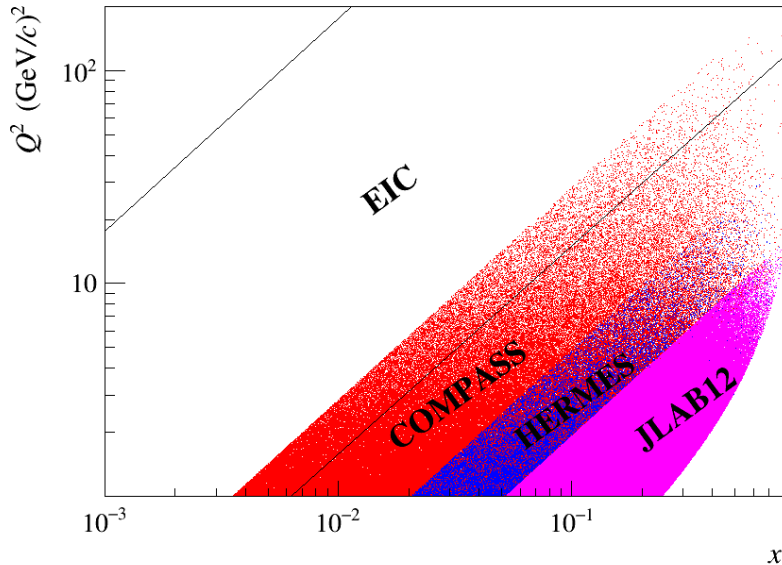
10

Figure 3: The $x - Q^2$ scatter plot for SIDIS experiments HERMES, COMPASS and JLab12. Also indicated are the ($\sqrt{s} = 140$ GeV , $y = 0.9$) and ($\sqrt{s} = 40$ GeV, $y = 0.1$) borders for a future EIC.

1.3.1 Present COMPASS data and extrapolated errors

The transversity PDF is chiral-odd and thus not directly observable in inclusive deep inelastic lepton-nucleon scattering. In 1993 Collins suggested [9] that it could be measured in SIDIS processes, where it appears coupled with another chiral-odd function, which by now is known as "Collins fragmentation function" $H_{1q}^{\perp h}$. It is the chiral-odd transverse-spin dependent FF that describes the correlation of quark (q) transverse polarisation and hadron (h) transverse momentum. This mechanism leads to a left-right asymmetry in the distribution of hadrons produced in the fragmentation of transversely polarized quarks, which in SIDIS shows up as an azimuthal transverse spin asymmetry A_{Coll} (the "Collins asymmetry") in the distribution of produced hadrons. At leading order this asymmetry can be written as

$$A_{Coll} = \frac{\sum_{q,\bar{q}} e_q^2 x h_1^q \otimes H_{1q}^{\perp}}{\sum_{q,\bar{q}} e_q^2 x f_1^q \otimes D_{1q}} \tag{2}$$

where the sum is over all (anti)quark flavours, D_q^h is the usual FF and $\otimes$ indicates the (different for numerator and denominator) convolutions over the intrinsic transverse momenta. The Collins effect shows up as a modulation $[1 + a_C \sin(\phi_h + \phi_S - \pi)]$ in the hadron azimuthal distribution. Here $\Phi_C = \phi_h + \phi_S - \pi$ is the Collins angle, and ϕ_h and ϕ_S are the azimuthal angles of the hadron transverse momentum $\boldsymbol{p}_{hT}$ and of the spin direction of the target nucleon with respect to the lepton scattering plane, in a reference system in which the z axis is the virtual-photon direction. The amplitude of the modulation is $a_C = D_{NN} f P A_{Coll}$, where D_{NN} is the transverse spin transfer coefficient from target quark to struck quark, f the dilution factor of the target material, and P is the proton (or deuteron) polarization. In Fig. 4 the results [12] for A_{Coll} we have obtained from the 2010 data collected using as target NH$_3$, a polarized proton target, are shown as a function of x and compared to the results we obtained [18] from the deuteron runs of 2002, 2003, and 2004, when as target we used ^{6}LiD.
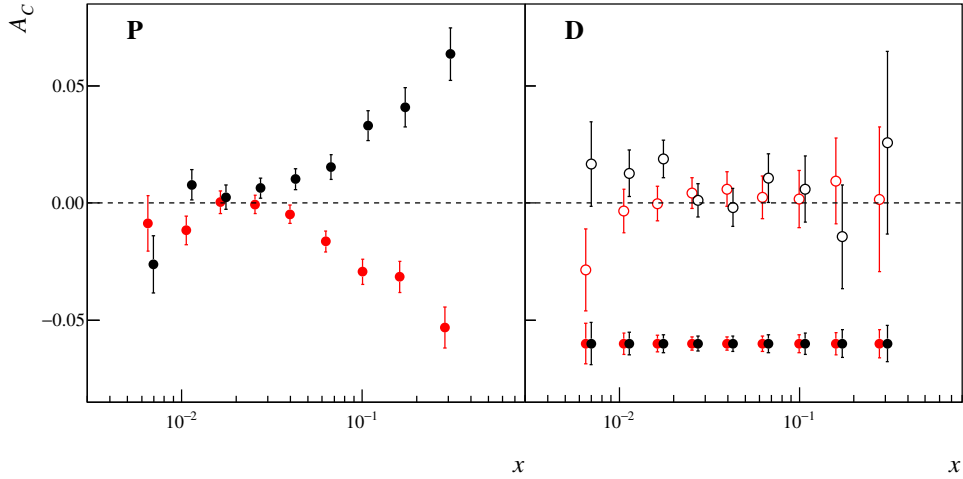
Figure 4: A_{Coll} obtained from the 2010 data with the polarized proton NH_3 target as a function of x (left plot) compared to the results we obtained [18] from the runs of 2002, 2003 and 2004 with polarised deuteron ^{6}LiD target (right plots). The red (black) points refer to positive (negative) hadrons. The full points at -0.06 in the right plot show the extrapolated statistical error from the proposed deuteron run (see text).

It is clear that the accuracy of the data is considerably better for the proton run, in particular at large x, where the Collins asymmetry is large. In order to quantify this fact, it is instructive to plot the ratio of the errors. In Fig. 5 this ratio is shown as a function of x. In order to understand this plot, one has to remind that, for small asymmetries, the statistical error is given by

$$\sigma_A \simeq \frac{1}{fP}\frac{1}{\sqrt{N}} = \frac{1}{FOM}\frac{1}{\sqrt{N}} \tag{3}$$
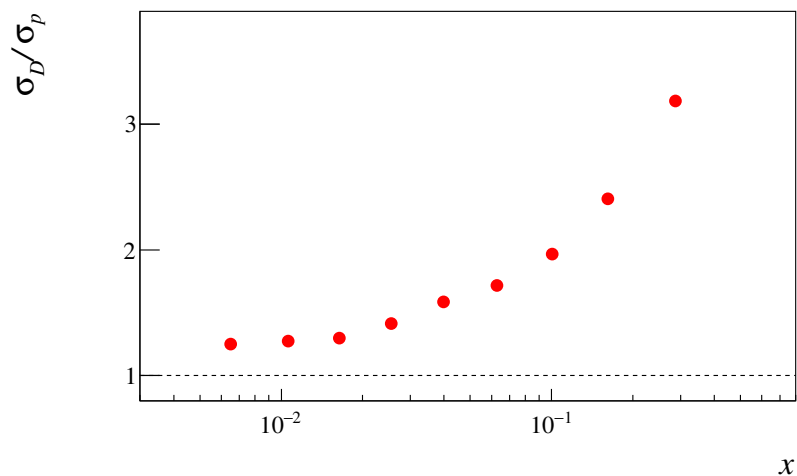

Figure 5: Ratio of the A_{Coll} statistical uncertainties on deuteron and proton.

where N is the total number of hadrons and FOM is the figure of merit of the polarised target. Using $N_{d,h} = 15.5 \cdot 10^6$ and $N_{p,h} = 80 \cdot 10^6$ as the values for the number of hadrons collected on p and d, and the known FOM values for the two targets, one gets

$$\frac{\sigma_{A_d}}{\sigma_{A_p}} = \frac{0.155 \cdot 0.80}{0.40 \cdot 0.50} \frac{\sqrt{80}}{\sqrt{15.5}} = 0.62 \cdot 2.3 = 1.4 \tag{4}$$

At small x, where most of the events cluster, the ratio between the deuteron and the proton asymmetries is indeed constant, since the spectrometer acceptance was essentially the same in the two data taking, and its value is close to 1.4. Here the better FOM of the deuteron target partly compensates the factor of 5 in statistics in favor of the proton target. The remaining 10% difference is due to the fact that the polarised target cells diameter in the deuteron runs was 3 cm while for the proton runs it was 4 cm, which resulted in a 20% larger beam acceptance in the proton runs. Our plan is to run in 2021 with 4 cm target cells diameter as long as enough ^{6}LiD material will be available. At large x on the contrary the ratio increases dramatically, reflecting the difference in acceptance of the COMPASS PT magnet, which has a polar angle acceptance of 200 mrad as seen from the upstream end of the target, while in the earlier measurements with the ^{6}LiD target we had utilized the SMC magnet, which has a corresponding polar angle acceptance of 70 mrad.

1.3.2 Projected errors after 1 year of deuteron run

Since target density and packing factors are essentially identical for ^{6}LiD and NH_3, it can be safely assumed that in one year of deuteron run in the conditions of the 2010 proton run $80 \cdot 10^6$ "good" events will be collected, so that the errors on the new deuteron asymmetries will be equal to the present errors for the 2010 proton asymmetries scaled by the ratio of the FOM, namely they will be smaller by a factor of 0.62. The projected errors for the deuteron asymmetries are also plotted in Fig. 4, together with the existing deuteron and proton asymmetries. We neglect the systematic errors which were estimated to be at most 0.5 times the statistical errors in the 2010 data. Using the 2010 proton data and the projections of Fig. 4 for the new deuteron data it is possible to extract the u- and d-quark transversity, and quantify the gain in statistical error in these fundamental PDFs. To carry through this evaluation we have followed the procedure of Ref. [21], which allows a point by point extraction of transversity directly from the measured SIDIS and $e^+e^- \rightarrow hadrons$ asymmetries. The results of such extractions are given in Fig. 6, which shows both the values of transversity (open points) extracted from the existing p and d data, and the corresponding error bars (closed points) estimated using the existing p data and the new d data. Also, Fig. 7 gives the ratio, at each x value, of the existing errors on the extracted transversities and the projected errors, taking the existing proton asymmetries from 2010 and the projected errors for the deuteron asymmetries obtained after 1 year of running. One can see that the gain in precision is quite good for the d-quark and important also for the u-quark.

1.3.3 Projections for the tensor charge

In order to evaluate the tensor charge it is convenient to introduce a functional dependence for h_1^q, to be fixed by fitting the extracted values of $xh_1^{u_v}$ and $xh_1^{d_v}$. We neglect the Q^2 dependence of h_1 and take

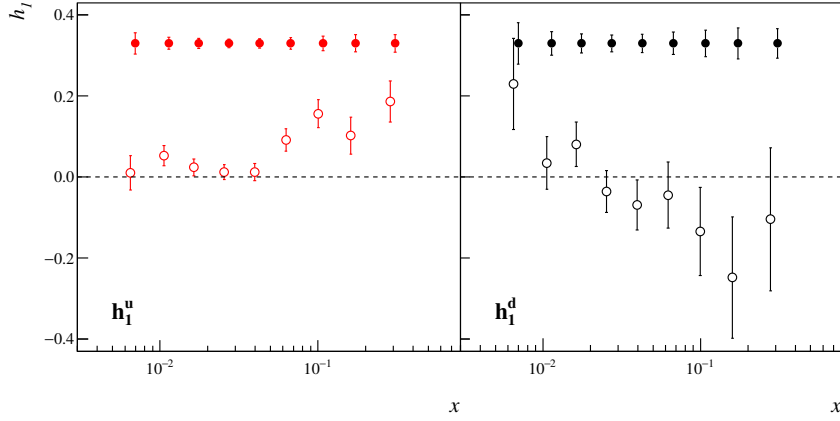$$xh_1^q(x) = a_q x^{b_q}(1-x)^{c_q}. \tag{5}$$

Figure 6: Values of u_v-quark (left) and d_v-quark (right) transversity extracted from the existing p and d data (open points), and the corresponding error bars estimated using the existing p data and the new d data (closed points).
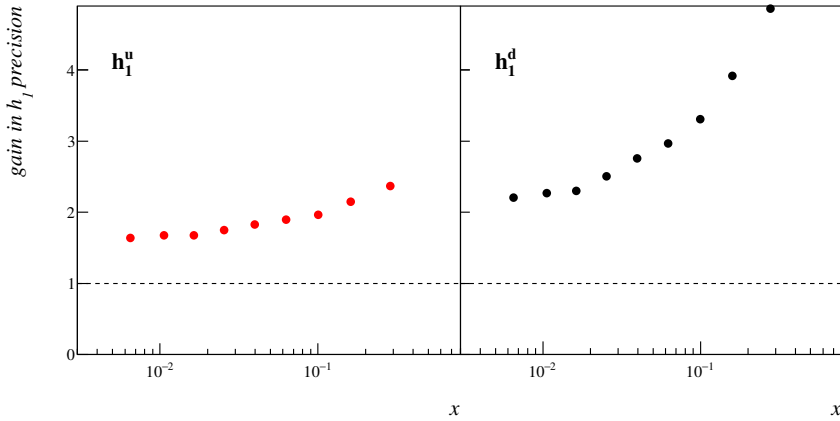

Figure 7: Ratio of the existing errors on the extracted transversities and the projected errors for u_v-quark (left) and d_v-quark (right).

Unfortunately, the present statistical accuracy on xh_1^q with $q = u_v, d_v$ does not allow to safely determine all the parameters a_q, b_q and c_q and in particular their covariance matrix, needed for this exercise. We thus assumed $c_q = 4$, as suggested by the central values given by the fit. For the remaining two free parameters we get

$$a_{u_v} = 3.5 \pm 1.6, \; b_{u_v} = 1.3 \pm 0.2, \; a_{d_v} = -5.2 \pm 5.3, \; b_{d_v} = 1.5 \pm 0.5 \,. \tag{6}$$

The comparisons between the fitted $xh_1^{u_v}$ and $xh_1^{d_v}$ and the extracted transversity values are shown in Fig. 8, together with the 68% uncertainty bands.

To estimate the impact of our measurements on the extraction of the tensor charge, the curves have been numerically integrated in the full range $0 < x < 1$ and the measured range $0.003 < x < 0.21$. The latter excludes our last measured x bin, in order to not overlap with the precise data from JLab12 which should come in the future. The results are given in Tab. 1 together with the corresponding value of $g_T = \int dx h_1^{u_v}(x) - \int dx h_1^{d_v}(x)$. While the evaluation of the d-quark tensor charge presently has no statistical significance, the new measurement should provide more than a 4σ effect with respect to the presently estimated value, and the extraction of g_T in the x-interval in which COMPASS can measure is more than respectable. For completeness we have
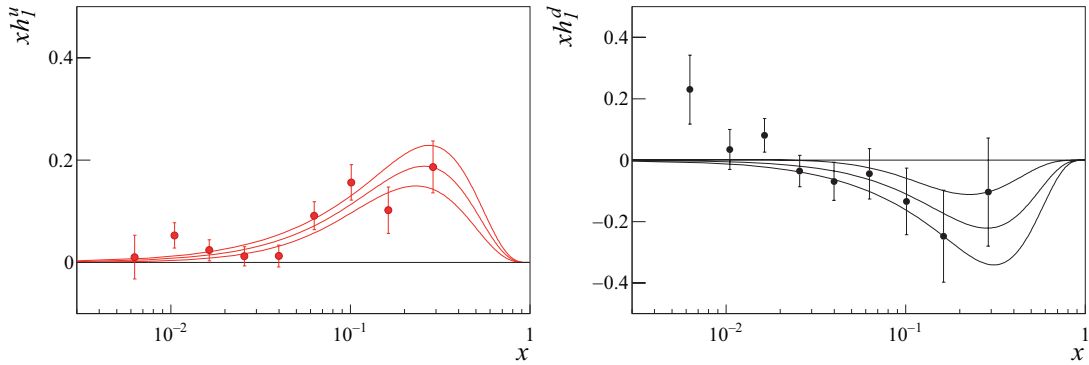
14

Figure 8: Extracted values of the valence quark transversity distributions $xh_1^{u_v}$ and $xh_1^{d_v}$ with the curves from the fits with the 1σ uncertainty band indicated.

Table 1: Integrated values of h_1 and result for g_T from the fits with the present and the projected uncertainties.

errors	$\int dx h_1^{u_v}(x)$	$\int dx h_1^{d_v}(x)$	g_T
	$0.003 < x < 0.21$		
old	0.255 ± 0.043	-0.202 ± 0.112	0.45 ± 0.12
proj	0.211 ± 0.027	-0.212 ± 0.042	0.423 ± 0.050
	$0 < x < 1$		
old	0.59 ± 0.13	-0.61 ± 0.35	1.20 ± 0.37
proj	0.587 ± 0.077	-0.585 ± 0.119	1.172 ± 0.142

integrated the fitted functions also in the entire domain $0 < x < 1$, to give an idea of the contribution that COMPASS can give to the determination of the tensor charge. Needless to say, this estimates are meant only to propagate the statistical uncertainties from the measured PDF to the integrated tensor charges in order to evaluate the impact of the new data, and not to give a value for the tensor charge itself.

1.4 Experimental Apparatus and Beam request

The apparatus to be used for the deuteron run is basically the COMPASS Spectrometer as it was used in the 2010 muon run. This implies removing the absorber which will be used for the 2018 Drell-Yan run, moving the polarised target 2 m downstream to the position it had for the SIDIS runs, and reinstalling all the trackers and all the counters which were used in 2010. The polarized target will be housed in the large acceptance COMPASS PT magnet, and the target material will be the same which was used in the years 2002, 2003, 2004 and 2006, namely ^{6}LiD. For a better usage of the muon beam, the target cells diameter will be increased from 3 to 4 cm. The average polarization of the target is expected to be the same as in the past deuteron runs ($\leq 50\%$).

The beam request is the same as for the 2010 proton run, namely 2.5×10^{13} protons delivered to the T6 target of the M2 beam line every 40.8 s. With an accelerator chain efficiency of 90% and a running time of 150 days a total of 6.1×10^{18} protons at T6 is expected. This number of protons is the basis of all the projections presented in this document, which are obtained from the number of reconstructed hadrons in the 2010 run.

The estimated uncertainties have been obtained assuming the COMPASS spectrometer availability and efficiency to be the same as in the 2010 run, but several upgrades

have already been implemented over the past years and more upgrades are foreseen for running after 2020. Tracking will profit of the addition of several trackers over the past ten years, in particular the new large area DC5, the pixelized GEMs and Micromegas and several scintillating fiber hodoscopes. At variance with the past deuteron runs, electromagnetic calorimetry will also be available (ECAL1 and ECAL2). Here we consider unidentified hadrons only, but as in 2010, particle identification will be provided by the RICH1 detector, for which the completion of the upgrade done for the 2016 run is foreseen. In addition some increase in the collected data is expected from hardware upgrades of the last years, in particular concerning the DAQ and trigger. Since no major upgrades of the present spectrometer are necessary for this measurement, it can start soon and take place in 2021.

1.5   Summary

We propose to improve our knowledge of the transverse spin structure of the nucleon by measuring 160 GeV muon semi inclusive DIS on a transversely polarized deuteron target. The proposed measurements will have a profound impact on the field, and their combination with the already taken proton data will allow to further clarify the properties of the up, down and sea quarks in the nucleon.

Quoting from our last proposal for a polarized SIDIS measurement [7], "the high intensity and polarization of the muon beam together with the COMPASS polarized target and spectrometer make CERN a unique place to perform such measurement. This will not change until the construction of a high energy and luminosity polarized electron-ion collider in the longer term future".

1.6   TMD PDFs and SIDIS scattering
from Ref. [7], App. A

The recent theoretical work on the nucleon structure points out the relevance of its transverse structure. A good knowledge of the transverse intrinsic momentum $\mathbf{k}_T$ carried by the partons and of its connection with the spin is needed to understand the parton orbital motion and to progress towards a more structured picture, beyond the collinear partonic representation.

In the QCD parton model, at leading twist, the nucleon structure is described by eight TMD PDFs: $f_1(x, \mathbf{k}_T^2)$, $g_{1L}(x, \mathbf{k}_T^2)$, $h_1(x, \mathbf{k}_T^2)$, $g_{1T}(x, \mathbf{k}_T^2)$, $h_{1T}^\perp(x, \mathbf{k}_T^2)$, $h_{1L}^\perp(x, \mathbf{k}_T^2)$, $h_1^\perp(x, \mathbf{k}_T^2)$ and $f_{1T}^\perp(x, \mathbf{k}_T^2)$, using the so-called Amsterdam notation. After integrating over $\mathbf{k}_T$ only the first three PDFs survive, yielding the number distribution $f_1(x)$ (or $q(x)$), the helicity distribution $g_1(x)$ (or $\Delta q(x)$), and the transversity distribution $h_1(x)$ (or $\Delta_T q(x)$ in the usual COMPASS notation). These three functions fully specify the quark structure of the nucleon at the twist-two level. Today, a lot of attention is put in particular on the TMD functions $f_{1T}^\perp$, the Sivers function which gives the correlation between the nucleon transverse spin and the quark intrinsic transverse momentum, $h_1^\perp$, the Boer–Mulders function which gives the correlation between the transverse spin and the intrinsic transverse momentum of a quark inside an unpolarised nucleon, and g_{1T}, which is the only chiral-even and T-even leading twist function in addition to f_1 and g_1.

A powerful method to access the poorly known TMD PDF is SIDIS on transversely polarised targets. In fact, on the basis of general principles of quantum field the-

ory in the one photon exchange approximation, the SIDIS cross-section in the COMPASS kinematical range can be written in a model independent way as:

$$
\begin{aligned}
\frac{d\sigma}{dx\,dy\,dz\,d\phi_S\,d\phi_h\,dp_T^h} \;=\; & \frac{\alpha^2}{xyQ^2}\frac{y^2}{2(1-\epsilon)}\Big\{F_{UU} + \\
& + \sqrt{2\epsilon(1+\epsilon)}\cos\phi_h F_{UU}^{\cos\phi_h} + \epsilon\cos2\phi_h\,F_{UU}^{\cos2\phi_h} + \\
& + \lambda\sqrt{2\epsilon(1-\epsilon)}\sin\phi_h F_{LU}^{\sin\phi_h} + \\
& + S_L\Big[\sqrt{2\epsilon(1+\epsilon)}\sin\phi_h F_{UL}^{\sin\phi_h} + \epsilon\sin2\phi_h F_{UL}^{\sin2\phi_h} + \\
& \qquad + \lambda\left(\sqrt{1-\epsilon^2}F_{LL} + \sqrt{2\epsilon(1-\epsilon)}\cos\phi_h F_{LL}^{\cos\phi_h}\right)\Big] + \\
& + S_T\Big[\sin(\phi_h-\phi_S)F_{UT}^{\sin(\phi_h-\phi_S)} + \epsilon\sin(\phi_h+\phi_S)F_{UT}^{\sin(\phi_h+\phi_S)} + \\
& \qquad + \epsilon\sin(3\phi_h-\phi_S)F_{UT}^{\sin(3\phi_h-\phi_S)} + \\
& \qquad + \sqrt{2\epsilon(1+\epsilon)}\sin\phi_S F_{UT}^{\sin\phi_S} + \\
& \qquad + \sqrt{2\epsilon(1+\epsilon)}\sin(2\phi_h-\phi_S)F_{UT}^{\sin(2\phi_h-\phi_S)} \\
& \qquad + \lambda\Big(\sqrt{1-\epsilon^2}\cos(\phi_h-\phi_S)F_{LT}^{\cos(\phi_h-\phi_S)} \\
& \qquad\qquad + \sqrt{2\epsilon(1-\epsilon)}\cos\phi_S F_{LT}^{\cos\phi_S} \\
& \qquad\qquad + \sqrt{2\epsilon(1-\epsilon)}\cos(2\phi_h-\phi_S)F_{LT}^{\cos(2\phi_h-\phi_S)}\Big)\Big]\Big\}. \quad (1)
\end{aligned}
$$

Here ϕ_S and ϕ_h are the azimuthal angles of the nucleon transverse spin and of the hadron transverse momentum $\boldsymbol{p}_T^h$ in the Gamma–Nucleon System, α is the fine structure constant, λ is the lepton helicity, S_T and S_L are the nucleon transverse and longitudinal polarisation. Neglecting the terms in $\gamma^2 = (2Mx/Q)^2$, the quantity ϵ is given by $\epsilon = (1-y)/(1-y+y^2/2)$.

The r.h.s. structure functions F's in general depend on Q^2, x, z and p_T^h. Their superscripts refer to the corresponding azimuthal asymmetries. The subscripts refer to the beam and to the target polarisation (U means unpolarised, L longitudinally polarised, and T transversely polarised). Since the modulations which appear in the cross-section for unpolarised, longitudinally polarised and transversely polarised nucleons are independent combinations of the azimuthal angles, all of them can be measured using data taken with unpolarised, longitudinally polarised and transversely polarised targets.

In the S_T-dependent part of the cross-section, only four of the eight structure functions are of leading order. They are:

- $F_{UT}^{\sin(\phi_h+\phi_S)} \propto h_1 \otimes H_1^\perp$, where h_1 is the transversity distribution, $H_1^\perp$ is the Collins fragmentation function and $\otimes$ indicates the convolution over the quark intrinsic transverse momentum summed over the quark flavors. When divided by F_{UU} it is the Collins asymmetry measured by COMPASS and HERMES;
- $F_{UT}^{\sin(\phi_h-\phi_S)} \propto f_{1T}^\perp \otimes D$, where $f_{1T}^\perp$ is the Sivers function and D is the unpolarised fragmentation function. When divided by F_{UU} it is the Sivers asymmetry measured by COMPASS and HERMES;
- $F_{UT}^{\sin(3\phi_h-\phi_S)} \propto h_{1T}^\perp \otimes H_1^\perp$, and
- $F_{LT}^{\cos(\phi_h-\phi_S)} \propto g_{1T} \otimes D$.

A complete list of the TMD PDFs which appear in all the structure functions can be found e.g. in Ref. [6]

2 Determination of the proton radius using high-energy μp scattering

2.1 Introduction

The determination of the size of the proton, the most abundant hadron in our Universe, has been in the focus of intensive research since more than 60 years [39](see Fig. 9 for the history of the proton charge radius). Unlike the protons' electric charge or its magnetic moment, which have been determined with high precision, the charge distribution of the proton and thus its mean square charge radius is badly known and has recently been at the origin of very active research programmes pursued at various laboratories. Traditionally, charge distributions are measured using low-energy elastic electron scattering. Measurements for the proton have partly made use of the Rosenbluth separation of the electric and magnetic form factors. The results of this method for the proton radius had been challenged about 7 years ago by high-precision muonic-hydrogen spectroscopy [40, 41] performed at PSI (see Fig. 10).
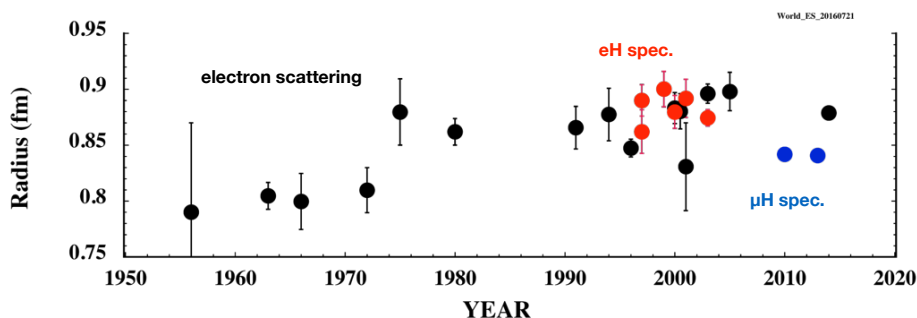

Figure 9: Historical development of the proton charge radius. Figure is taken from [42].

Despite much experimental efforts over the last years, the resulting proton radius puzzle [43] has plagued physicists ever since. At MAMI, an admirable experimental effort to address the proton radius using elastic ep scattering down to Q^2 of about $10^{-3}(\text{GeV}/c)^2$ has basically confirmed older electron scattering results [44]. These efforts were motivated by the suspicion, that the extrapolation of scattering data down to $Q^2 = 0$ might carry unknown uncertainties related to either experimental flaws of the measurements at higher values of Q^2 or by yet unknown physics changing the slope of the differential cross-section towards very small momentum transfers. New experiments are planned or under way [45], which aim at extending the lowest values of Q^2 down to $2 - 5 \cdot 10^{-4}(\text{GeV}/c)^2$ [46] (data taken in 2016)[47]. Here, detected initial state radiation is used to lower the range of Q^2 as compared to previous measurements at MAMI. Yet another experimental proposal at MAMI employs an alternative approach to determine Q^2 from the proton recoil alone (supplemented by the more standard measurement of the outgoing electron). Although the measurement uncertainties connected to electron scattering experiments are very different from those of spectroscopical results, the discrepancy in the proton radius determined by muonic hydrogen and ep elastic scattering is a multiple of this uncertainty.

Until recently, also the spectroscopy of electronic hydrogen differed from the muonic one, though by less than ep scattering data, and there has been a call to investigate the last missing experimental measurement, elastic μp scattering. Very recent spectroscopical data on muonic deuterium led to a new determination of the Rydberg constant ($R_\infty^{\mu d} = 3.289841960234(6) \cdot 10^{15}$ Hz/c, note there is a 2.2σ difference between $R_\infty^{\mu D}$ and $R_\infty^{\mu H}$) [49]. For this, atomic transitions to higher lying states ($2S \rightarrow nL$) had to be considered, which in case of electronic hydrogen led to inconsistent re-
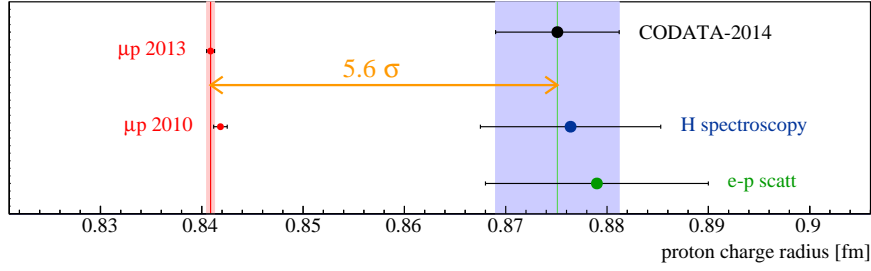
Figure 10: Proton charge radius from muonic hydrogen (red), hydrogen spectroscopy (blue) and electron-proton scattering (green). The CODATA value accounts for e-p scattering, H and deuterium (D) spectroscopy but does not consider the muonic results. Figure is taken from [48].

sults among various transitions. Averaging these results led to the Rydberg constant used to extract the proton radius from the Lamb-shift measurements ($2S \rightarrow 2P$) as $R_\infty^{\mathrm{CODATA-2010}} = 3.289841960355(19) \cdot 10^{15} \mathrm{Hz/c}$. The new determination of the Rydberg constant can be used to reinterpret all electronic hydrogen data, which now brings muonic and electronic hydrogen into agreement (there is a very strong correlation between the Rydberg constant and the proton radius from electronic hydrogen). This situation has now put more weight on the issue of lepton scattering versus spectroscopical radius measurements and quests for very low Q^2 data. Here, high energy muons are an ideal tool owing to reduced systematics from multiple scattering and Bremsstrahlung corrections.
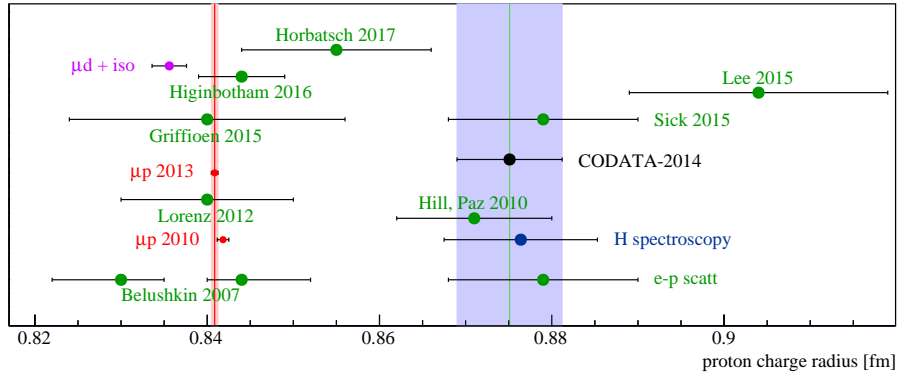

Figure 11: Proton radius from muonic hydrogen (red), hydrogen spectroscopy (blue) and electron-proton scattering (green). The CODATA value does not account for the muonic results. Figure is take from [48].

In addition to a very active discussion concerning the two different measurement methods there are debates on the proper analysis of electron scattering data. Bernauer and Distler, co-authors of the Mainz measurements, give a detailed explanation on the techniques of model fitting on the electron scattering data [50], firmly concluding to the large value for the proton radius. On the other hand, [51, 52] argue from a theoretical point of view on the unphysical parametrisation of form factors used by the experimentalists, leading to a false slope of the form factors at $Q^2 = 0$. Indeed, their fit of the electron scattering data using a dispersive approach for the form factors results in proton charge radius very well compatible with the spectroscopical data. The multitude of fit

19

results using various ranges in Q^2 and fit functions is shown in Fig. 11. Some analyses are compatible with the muon spectroscopic value and some are at variance. The more traditional analyses obtain values for the charge radius systematically larger than obtained by other authors that restricted the momentum transfer to very low Q^2 and used low-order power series. Possible issues of fits restricted to very low Q^2 have been demonstrated by analyzing pseudo-data generated with known proton radius (see [48] for more details).

The present situation asks for a new measurement using a different experimental ansatz and covering a wide range of Q^2. The low Q^2 region is vital to constrain the parametrisation of the form factors and thus gives more comfort for their extrapolation to $Q^2 = 0$. A lower limit of $Q^2 = 10^{-4} \, (\text{GeV}/c)^2$ is desirable. On the other hand, the region of somewhat larger Q^2 gives more sensitivity to the charge radius.

The MUSE [53] experiment at PSI has recently been set-up to perform a first precision experiment on elastic μp scattering, investigating with the same apparatus elastic scattering of positive and negative muons, electrons and positrons. As these measurements are performed at very low Q^2, beam intensity is not an issue, unlike for form factor measurements at high Q^2, where high-intensity electron beam machines like JLab or MAMI are without alternative. The PSI experiment MUSE aims at accuracies, which are compatible with older electron beam data, which is mainly caused by the low μ-beam energies at PSI. The kinematic range in Q^2 for MUSE is $0.0016 - 0.0799 \, (GeV/\text{c})^2$ and is almost the same for electrons and muons. The largest uncertainties from this measurement will come from muon decay corrections (before or after the scattering process) and radiative corrections. The statistical uncertainties of the cross-sections range from about 0.3% to 1% at the larger scattering angles. The systematic uncertainties are at about the 0.5% level, thus systematic uncertainties are expected to slightly outweigh statistical ones. For each particle species they thus expect an accuracy of their measurement of 0.01 fm for the radius, possibly even 0.006 fm, depending on the analysis method.

The μ beam flux at PSI varies between $0.2 - 6 \cdot 10^6/s$ and is beam charge and energy dependent. It is typically below the time-averaged muon beam intensities achieved at COMPASS. While at COMPASS the μ-beam is pure at the level of $10^{-5} - 10^{-6}$ on what concerns pion contamination, electrons constitute the largest background for MUSE being a factor $10 - 100$ more abundant than muons. Similar numbers hold for pion background.

Very recently, a new experiment has been proposed at Tohoku Univ. (Japan) aiming at very low energy scattering of electrons from protons in order to address the smallest region of $Q^2 > 0.0003 \, (\text{GeV}/c)^2$. Electron beam energies between $20 - 60$ MeV are planned impinging on a hydrogen target with carbon admixture for luminosity measurements.

2.2 A μp elastic scattering experiment at COMPASS

In light of the experimental situation outlined above, it seems desirable, to perform a highly competitive elastic proton scattering measurement with high energy muons within the COMPASS experiment at CERN, which combines most of the above mentioned improvements of individual experimental efforts.

- a high intensity muon beam
- a high energy beam for low multiple scattering effects
- easy beam charge flips to measure both μ^+ and μ^- scattering
- high resolution in Q^2 of a few $10^{-4} \, (\text{GeV}/c)^2$, as demonstrated by pion Primakoff scattering [54]
- employment of an active target, to allow for precise proton recoil measurement

- possibly reference measurements to prove control of the experimental luminosity (e.g. μe elastic scattering)
- possibility to employ a high energy electron beam at the same beam line (details to be investigated)[55]

2.2.1 Kinematics

The differential Mott cross-section for elastic lepton scattering on nucleons is given by [56]:

$$\frac{d\sigma}{dt} = \frac{4\pi\alpha^2(\hbar c)^2}{t^2}\left\{\left[\frac{(s+M^2-m^2)^2}{4M^2-t}+m^2-s\right]\left[4M^2G_E^2(Q^2)-t\;G_M^2(Q^2)\right]\right.$$
$$\left.+t\left(m^2+\frac{t}{2}\right)G_M^2(Q^2)\right\}\frac{1}{s-(M+m)^2}\;\frac{1}{s-(M-m)^2} \tag{2}$$

where $t = -Q^2$ is the momentum transfer squared and s is the centre-of-mass energy squared. Target and beam particle masses are denoted by M and m, respectively. In the cross-section the finite size of the nucleon is characterised by the electric and magnetic form factors $G_E(Q^2)$ and $G_M(Q^2)$. At small values of four-momentum transfer these form factors are typically written in terms of the nucleon electric charge radius r_e expanded in powers of Q^2 [50]:

$$G_E(Q^2)/G_E(Q^2=0) = 1 - \frac{1}{6}\langle r_e^2\rangle\;Q^2 + \frac{1}{120}\langle r_e^4\rangle\;Q^4 - \frac{1}{5040}\langle r_e^6\rangle\;Q^6 \tag{3}$$

and the mean of the charge-radius squared can be extracted from the slope of the form factor at zero Q^2:

$$\langle r_e^2\rangle = -6 \cdot \left.\frac{dG_E(Q^2)}{dQ^2}\right|_{Q^2=0} \tag{4}$$

The Q^2 dependence of the cross-section is shown in Fig. 12a. As the expansion of the form factors in terms of $\langle r_e^2\rangle$ is only working for small values of Q^2, we also show the differential cross-section using the dipole form-factor[2] up to larger values of Q^2 Fig. 12b. The sensitivity of the cross-section for different values of the charge radius is depicted in Fig. 13, where we show the cross-section ratio for two extreme values of $\sqrt{\langle r_e^2\rangle}$ with 0.84 fm and 0.88 fm. Although it is assumed that measuring down to very small values of Q^2 reduces uncertainties extrapolating the measured cross-section down to $Q^2 = 0$, sensitivity to finite size effects can only be obtained at higher values of Q^2.

2.2.2 Requirements deduced from scattering kinematics and cross-section

In order to design the experimental set-up we need to understand the scattering kinematics. Figures 14 and 15b show the Q^2 dependence of energy and scattering angle of the scattered muon, Figs. 16 and 17 the corresponding distributions for the recoil proton. For the proton the polar scattering angle is calculated w.r.t. the normal of the incoming beam. In elastic scattering, recoil energy and angle are correlated and are shown in Fig. 18. All kinematic quantities only depend on Q^2 and are almost independent of the beam energy, except for the muon scattering angle shown in Fig. 15a for three different possible values of the incoming muon energy.

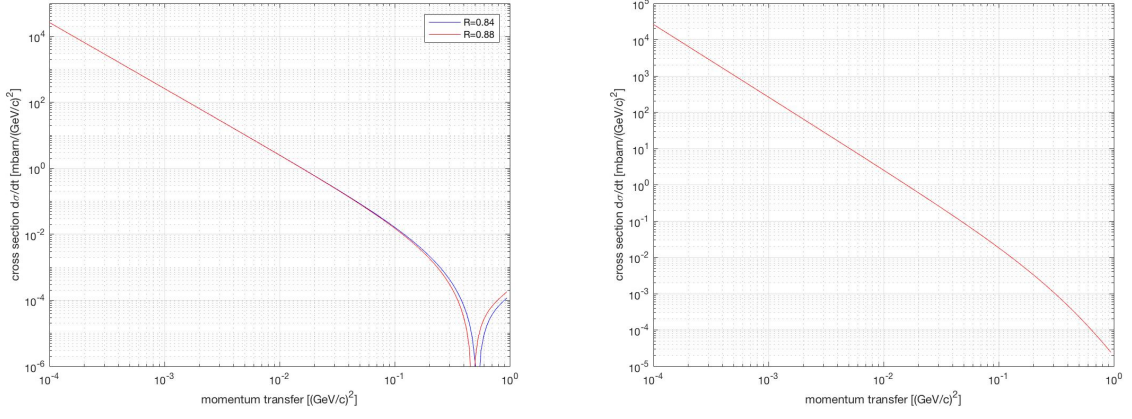[2] $G_{E,M} = (1 + Q^2/(0.71(\text{GeV}/c)^2))^{-2}$

Figure 12: Q^2 dependence of the μp elastic scattering cross-section for different form factor parametrizations. Left: form factor expansion in powers of Q^2 and $\sqrt{\langle r_e^2 \rangle}$ (see Eq. (3)) assuming a $\sqrt{\langle r_e^2 \rangle}$ of 0.84 fm and 0.88 fm. Right: assuming a dipole form-factor (see text).
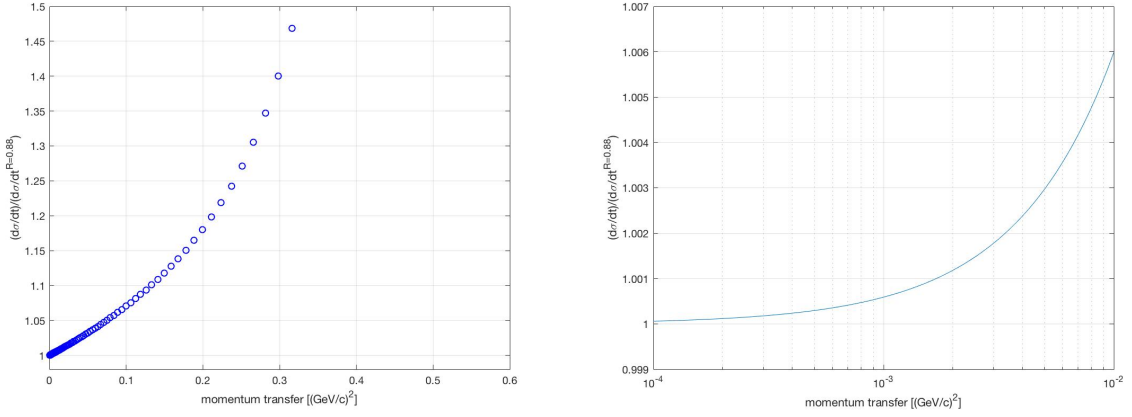

Figure 13: Ratio of cross-sections for $\sqrt{\langle r_e^2 \rangle}$ with 0.84 fm and 0.88 fm (denoted as σ_0) according to Eq. (3). Left: for large values of Q^2 (linear scale), right: zoom for low Q^2 (semi-log scaling).
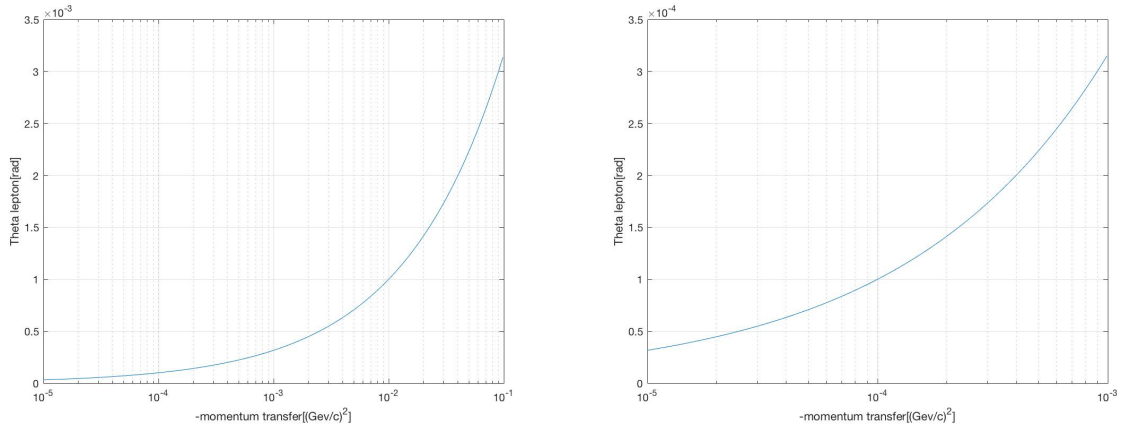
Figure 14: Q^2 dependence of the muon scattering angle for elastic μp scattering assuming 100 GeV beam energy
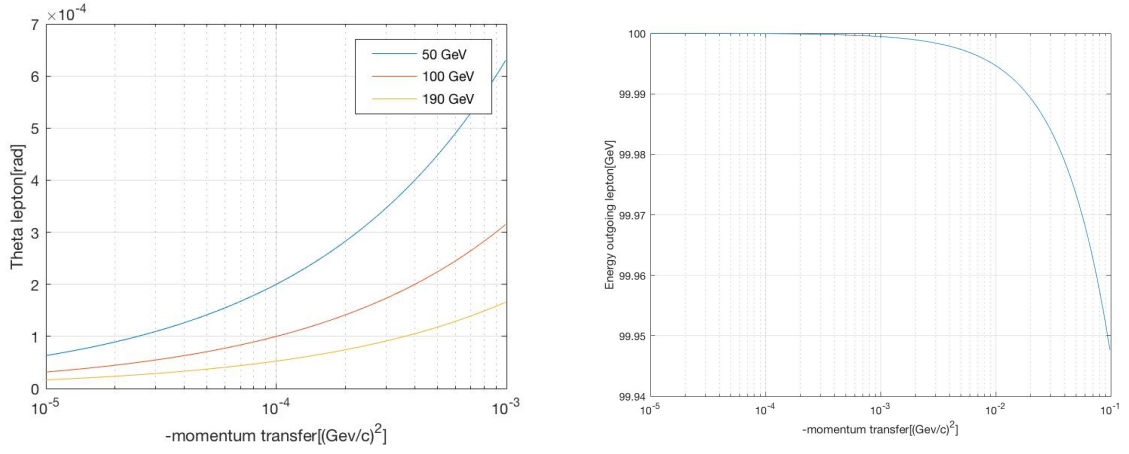
Figure 15: Left: Q^2 dependence of the muon scattering angle for elastic μp scattering assuming three different beam energies of 50, 100 and 190 GeV. Right: Q^2 dependence of the energy of the outgoing muon assuming 100 GeV beam energy.
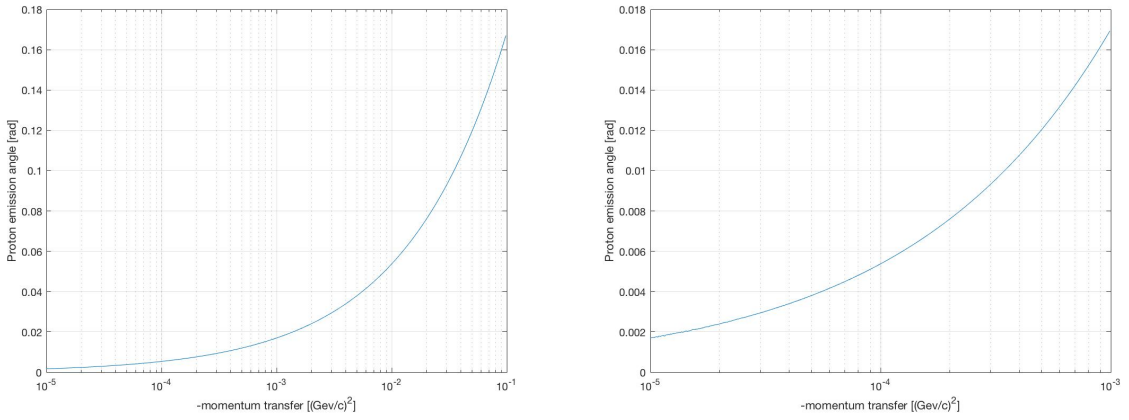
Figure 16: Left: Q^2 dependence of the proton polar scattering angle (measured w.r.t. the normal of the beam direction) for elastic μp for different intervals of Q^2.
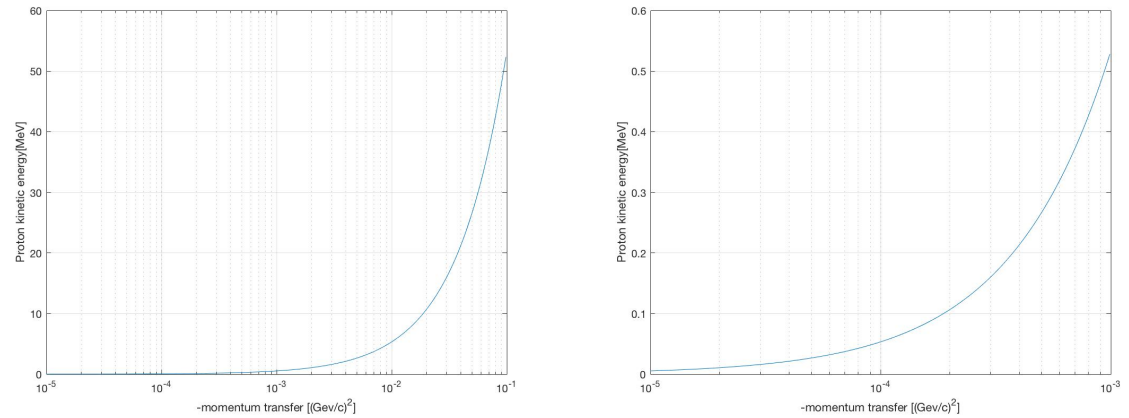
Figure 17: Q^2 dependence of the energy of the outgoing proton assuming 100 GeV beam energy for different intervals of Q^2.

23

Figure 18: Correlation of proton emission angle (measured w.r.t. the normal of the beam direction) and proton kinetic energy.

At a beam energy as large as 100 GeV typical magnetic spectrometers have energy resolutions of a few ‰ being insufficient to determine Q^2, which thus has to be determined from the muon scattering angle alone. However, scattering angles are small and typical far below the beam divergence. This imposes new triggering schemes in order to reach values for $Q^2 \approx 10^{-4}\,(\mathrm{GeV}/c)^2$.
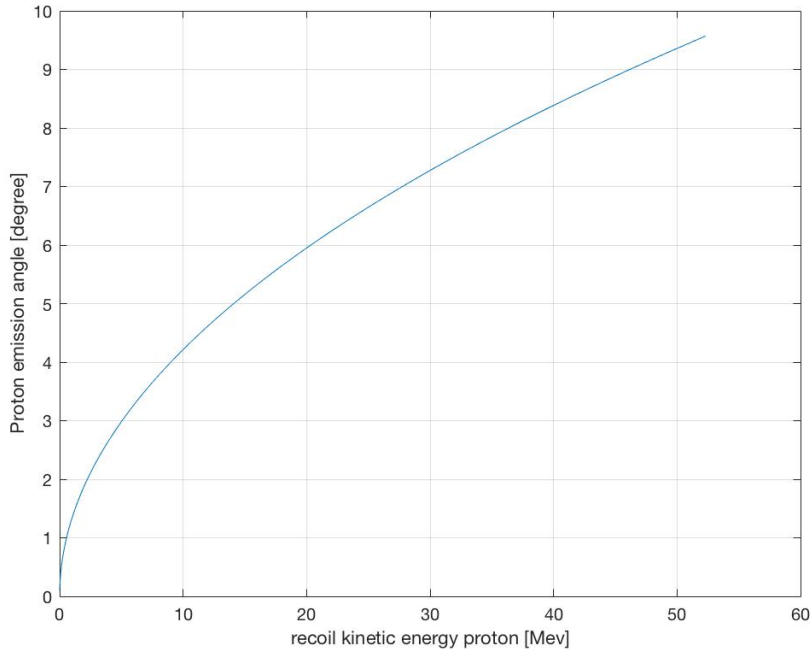
The recoil proton is emitted mostly perpendicular to the beam at about 90° and reaches 10° with respect to the beam normal for higher values of $Q^2 \approx 10^{-1}\,(\mathrm{GeV}/c)^2$. Small values of Q^2 result into small proton energies where the determination of the emission angle will be difficult. Thus, the measurement of the recoil angle cannot be used to determine Q^2 or act as a trigger signal. However, the proton recoil energy varies from 50 keV to 50 MeV for $10^{-4} < Q^2 < 10^{-1}\,(\mathrm{GeV}/c)^2$. It may thus be used as secondary measurement of Q^2 for most of the range of interest.

2.3 Experimental set-up

The experimental set-up uses the standard muon beam set-up of COMPASS, but the target region will be modified as to accommodate an active hydrogen target, possibly an active SciFi target and two silicon telescopes. It is depicted in Fig. 19. The active hydrogen target (ICAR [57]) is based on an existing set-up used for an experiment at GSI, which is shown in Fig. 20. Such a system has been developed by the Gatchina group (PNPI), and has been employed for multiple radius measurements in the past.

2.3.1 Proton recoil measurement

The proton recoil measurement can be achieved using a double target scenario. For small values of Q^2, with proton kinetic energies up to a few MeV, we can use a high
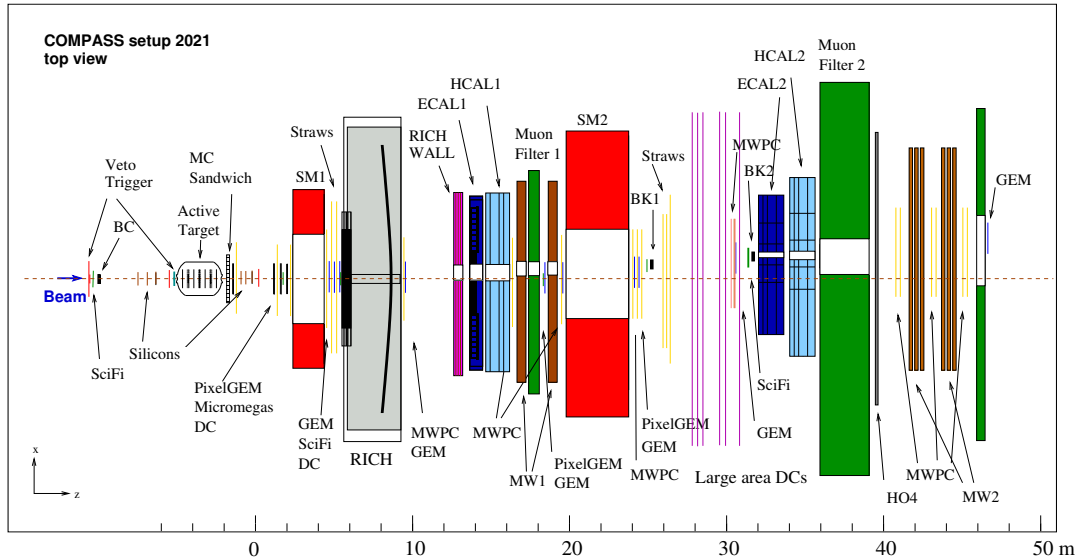
Figure 19: Schematics of the COMPASS MUP set-up. The target region including the gaseous hydrogen TPC is not to scale.
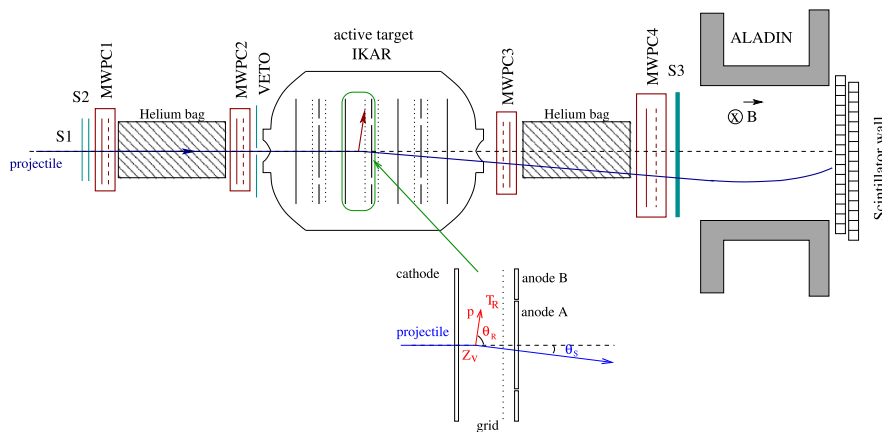
Figure 20: Example for the use of a high pressure active target TPC [57]

pressure hydrogen TPC operated as ionisation chamber. At higher values of Q^2 one may envisage an active target made from scintillating fibres.

2.3.2 A pressurised hydrogen-filled ionization TPC

Since the very beginning of elastic scattering experiments with leptons, high-pressure, thin-wall gas chambers were used as targets, the design of which was pioneered by Eva Wiener[3]. An example for an experiment using such a device is shown in Fig. 20 [57]. Such targets have been turned into an active target/detector system by the Gatchina group (PNPI) [58], and have been employed for multiple radius measurements in the past. The energy dependence of the specific energy loss and range for recoil protons in hydrogen gas at a working pressure of 4 bar are shown in Fig. 24. The energy dependent specific energy loss for the muon is shown in Fig. 26. The energy loss for incoming and outgoing

---

[3] a PhD student of R. Hofstadter who died in a car accident during her thesis work

Figure 21: Sketch of the target TPC with pressure vessel as conceived for an elastic e^-p scattering experiment at MAMI. The forward tracker system on the right side of the vessel will not be installed for COMPASS.

muons is about 2 keV/cm and thus small as compared to the proton energy loss even for proton kinetic energies of 10 MeV, as long as the path length traversed is below 10 cm.

For $Q^2 = 10^{-4} \, (\text{GeV}/c)^2$, the kinetic energy of recoil protons is $50-60$ keV. This value corresponds to the energy resolution obtained by [58] in an experiment measuring πp scattering 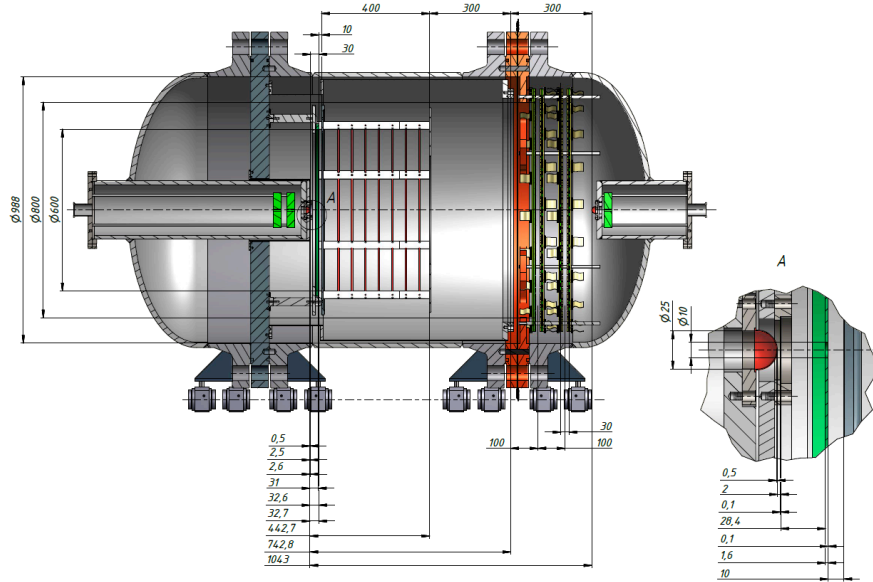in the Coulomb-nuclear interference region. This roughly determines the scale for the lowest value of Q^2 in the experiment.

A key issue for the TPC is the maximal drift time. This determines the effective gate length and thus the overlay of non-interacting beam particles.

The 60 cm long hydrogen-gas volume is divided into slices of 20 cm, each one forming a TPC with drift in longitudinal (beam) direction. Unlike in most other cases the TPC will be operated in ionisation mode. This avoids statistical fluctuations in the amplification process and thus allows for high energy resolutions. The latter is only determined by fluctuations in the primary ionisation. Resolutions of 50 keV have been obtained in NA8 at beam intensities of 10^6. The design of the TPC is motivated by the exact knowledge of the fiducial volume for reconstructable elastic scattering events. This requires high precision on the gas density and geometrical parameters, the exact characterisation of the active TPC volume. Details on the construction and calibration of the TPC can be found in Section 2.13. Figure 21 shows a sketch of the target vessel with the integrated system of TPCs.

Resolutions

As the hydrogen gas volume is segmented into 3 independent TPC sections we need to identify the TPC section for the scattering. The longitudinal vertex resolution using the scattered muon alone is sufficient for $Q^2 > 4 \cdot 10^{-3} (\text{GeV}/c)^2$, as can be seen in Fig. 22. Measuring smaller momentum transfers requires the information from the recoil proton measured within the TPC. This can be done requiring a minimum energy deposit detected in a TPC segment of $> 3 \cdot \sigma_{noise} = 150 - 200$ keV. Using more sophisticated algorithms

considering the pulseheight pattern observed in all TPC segments could possibly lower this limit, which however ist not crucial for this measurement.
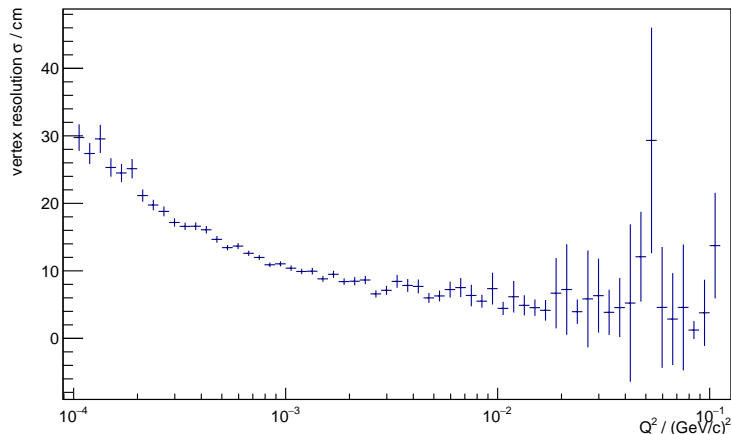

Figure 22: Longitudinal vertex resolution σ_z for a reconstruction only based on incoming and scattered muon.

We have performed first simulations on the achievable Q^2 resolution using the ionisation TPC. The results are shown in Fig. 23. We assume the set-up for the target region depicted in Fig. 23a. Each silicon station is assumed to be of the type used for Primakoff measurements performed previously by COMPASS. However, the spacing of the stations has been enlarged to 1m for both beam and spectrometer telescopes. In Fig. 23b) we show the achievable relative Q^2 resolutions for different values Q^2. For silicon alone, we use the standard COMPASS track reconstruction algorithms. For the Q^2 reconstruction within the TPC we assume an energy resolution for the kinetic recoil proton energy of 60 keV. We also show the results for the combined reconstruction. We conclude that we can perform measurements for elastic μp scattering down to $Q^2 \approx 10^{-4}$ $(\mathrm{GeV}/c)^2$.

2.3.3 An active scintillating fibre target

To motivate accessing higher values of Q^2 we refer to a study by [43] on the influence of the statistical error on the proton radius extracted from electron scattering data for different cut-offs in Q^2_{max} (see Fig. 27). Although the details refer to a particular set of data points from the MAMI measurement it demonstrates the strong influence of high Q^2 in the fit.

For higher values of Q^2 we envisage to use an active target made from scintillating fibres arranged vertically to the beam direction. These fibres cover the central beam area and have an effective thickness in beam direction of 1 cm. They are staggered in 3D as to minimise obscuring the recoil detector and thus reducing solid angle. The target fibres are surrounded by longitudinally stretched fibres arranged on a cylinder along the beam direction forming the proton recoil detector. Consecutive layers are arranged in a relative stereo angle of 6° . A possible set-up is shown in Fig. 29. The scintillation light from the fibres is detected on one side by SiPM of high pixel density (Hamamatsu S13360-3025 or KETEK PM3325) to reduce saturation effects. The backend opposing the SiPM is aluminised. In the model used for simulation we assumed 10 layers of scintillating fibres, summing up to $2-3$ cm thickness. In order to perform a combined $(dE/dx, E)$ analysis,

27

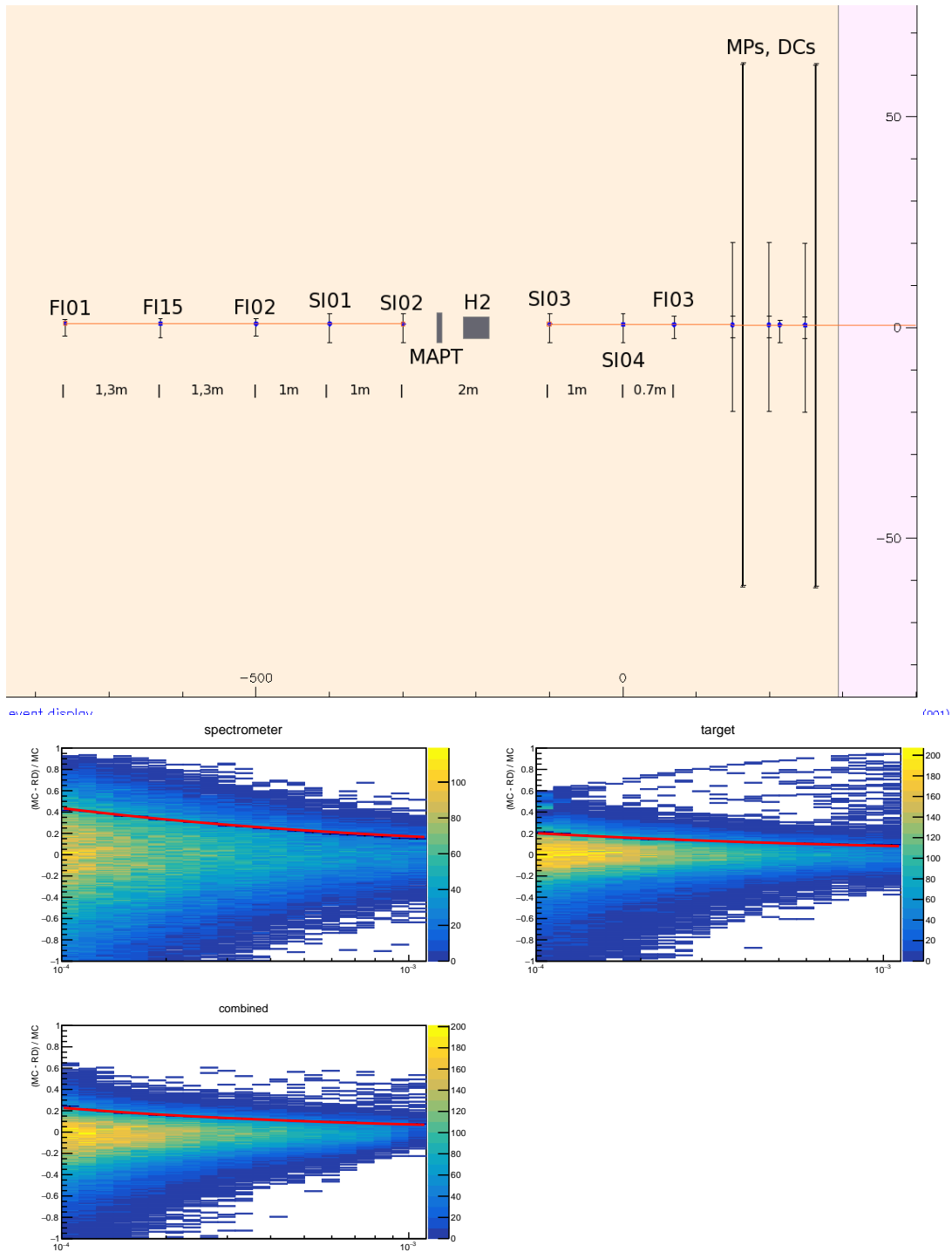Figure 23: Top: set-up of the target region used for resolution studies. Downstream of this region, the full standard COMPASS spectrometer is assumed. Right: Projected relative Q^2 resolutions using two silicon telescopes and an ionisation TPC fill with hydrogen gas at 4 bar pressure. The contribution from each detector is shown separately as well as the combined information. The mean values are shown as red lines.

28
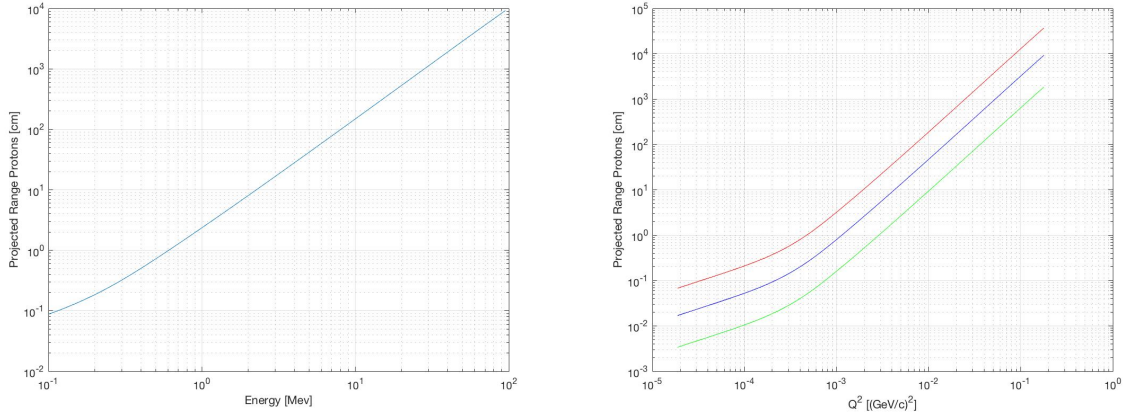
Figure 24: Projected range for protons in hydrogen gas. Left: hydrogen at 4 bar pressure for different kinetic energies [59]. Right: in hydrogen at 1 bar (red), 4 bar(blue) and 20 bar(green) for different Q^2.
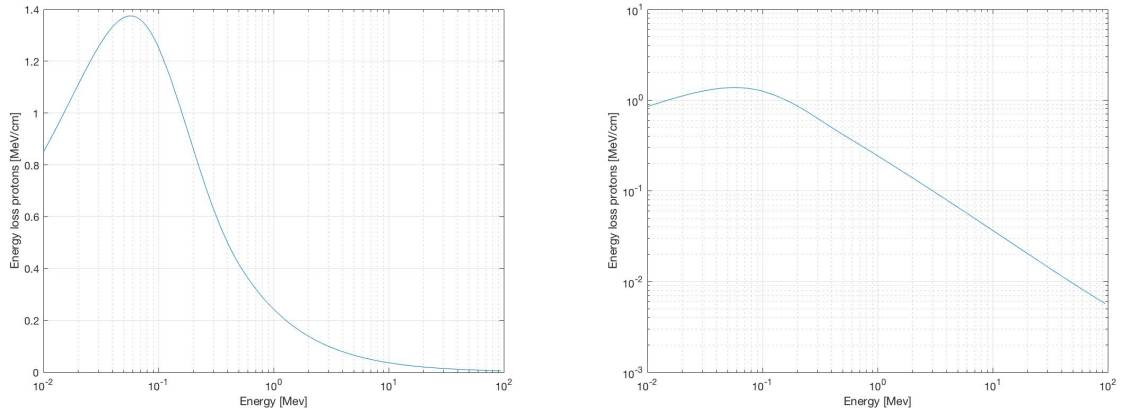
Figure 25: Projected range (left) and specific energy loss (right) for protons in hydrogen gas at 4 bar pressure for different kinetic energies [59].

we intend to surround the fibre tracker by 8 plates of scintillator, similar to the proton recoil detector surrounding the liquid hydrogen target of COMPASS in 2009. With this, we should be able to stop protons up to 100 MeV. Figure 28 shows both range and specific energy loss of protons in scintillator made from vinyltoluene-based material. By reconstructing the Bragg curve (Fig. 30a) we can obtain energy resolutions in the range of percent (Fig. 30b). We have performed test measurements on energy resolution up to energies of about 50 MeV at PSI using various fibre material and models of SiPM. Results from the analysis are expected soon.

As the range of low energy protons in the SciFi material is low we need to keep the fibre thickness small in the inner layers ($2 \times 2\,\mathrm{mm}^2$ or thinner). A requirement for the recoil proton of crossing at least 2 fibres to determine a 3D impact point imposes a lower limit for the kinetic energy of recoil protons of about 15-20 MeV. This corresponds to a lower value of $Q^2 > 0.03 - 0.04\,(\mathrm{GeV}/c)^2$, as can be read from Fig. 17. The fibre cross-section for the outer layers may grow to $4 \times 4\,\mathrm{mm}^2$ and $8 \times 8\,\mathrm{mm}^2$.
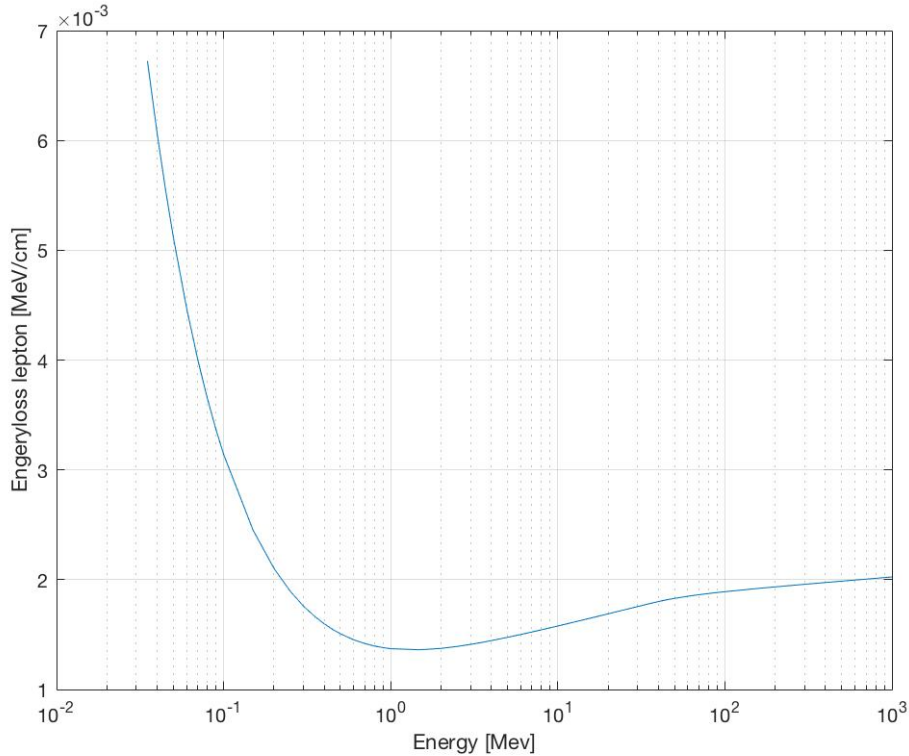
Figure 26: Specific energy loss for muons in hydrogen gas at 4 bar pressure for different kinetic energies [59].

For the present rate studies, we have assumed a total thickness of the target fibres in beam direction to be $1\,\mathrm{cm}$, in order to reduce multiple scattering. Assuming a fibre cross section of $1 \times 2\,\mathrm{mm}^2$ with the $2\,\mathrm{mm}$ side in beam direction we need about 500 fibres to cover the beam region of $1 \times 1\ \ \mathrm{cm}^2$. With the instantaneous beam intensity of about $5 \cdot 10^7\,\mu/\mathrm{s}/\mathrm{cm}^2$ the individual rates per fibre are about $5 \cdot 10^5\,\mu/\mathrm{s}/\mathrm{fibre}$. As SiPM and connected electronic circuitry have a dead time of about $200\,\mathrm{ns}$, this should reduce dead time corrections (one might further decrease the dead time with suitable shapers for the preamps.).

The use of a solid target infers quasielastic scattering events to spoil the data sample. However, they constitute a partly reducible background. Owing to the quasi elastic kinematics, good energy and angular resolution for the recoil proton is mandatory to allow for a rejection by about a factor 100 up to $Q^2 < 0.2 - 0.3\,(\mathrm{GeV}/c)^2$. Considering a SciFi composition of $(\mathrm{CH})_n$, the quasi elastic background would be six times higher than the elastic signal. As the cross section for the two different radii considered is about 10-20% above $Q^2 > 0.1\,(\mathrm{GeV}/c)^2$ as depicted in Fig. 31b), this limits the accessible range of such a measurement.

The readout of SiPM can be performed using a TDC ASICs (CLARO-CMOS developed for the upgraded LHCb RICH detector) or IDE3380 SIPHRA (developed for SiPM in space usage) and performing a time-over-threshold analysis. Performance tests are ongoing for a similar project. We will also derive a fast digital signal for triggering using a dedicated FPGA logic.
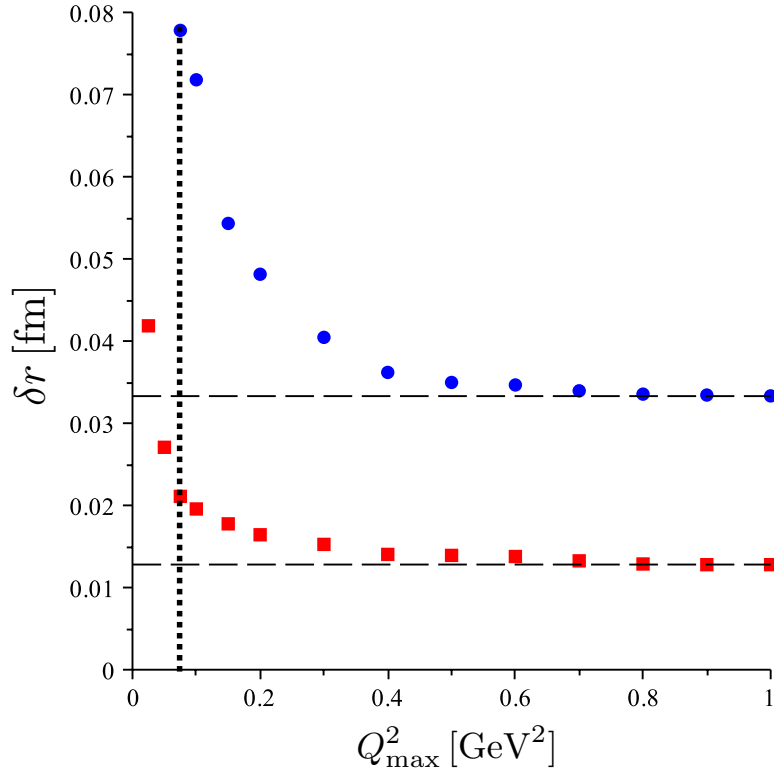
Figure 27: Statistical uncertainty on the proton charge radius as a function of the maximum momentum transfer retained in the fit, Q^2 max, for the 1422 point A1 MAMI dataset (red squares) and for the complementary world cross section and polarisation dataset (blue circles). The horizontal dashed lines are large-Q^2_{max} asymptotes. The vertical dotted line represents the limit $Q^2_{max} = 4m^2_\pi$ beyond which the two-pion threshold introduces non-analytic structure. Graph taken from [43]. See also references therein.

The geometry of the fibres target has not yet been optimised in terms of geometry, fibre cross sections and number of channels. However, the arrangement sketched up is feasible and has a reasonably flat acceptance across Q^2. Optimisation should allow to further reduce an unwanted Q^2 dependence of the acceptance and allow to obtain an effective threshold of $Q^2 > 0.3 \, (\text{GeV}/c)^2$.

2.4   Muon measurement

The scattered muon can be identified using the COMPASS spectrometer including the present muon identification system. As mentioned above, the energy transfer in the reaction is very small and falls within the energy resolution of the spectrometer. However, COMPASS has proven excellent angular resolution in the context of a measurement scattering pions of 190 GeV energy off the electromagnetic field of heavy nuclei like Pb or Ni [54]. Despite the presence of a solid target of thickness d = $20\% X_0$, COMPASS obtained a Q^2-resolution of $\Delta Q^2 = 2 \cdot 10^{-4} \, (\text{GeV}/c)^2$. This was achieved by means of two silicon telescopes placed upstream and downstream of the solid target. The position resolution of each silicon station was about $\Delta x \approx 4 \mu$m. In this set-up, we propose to position the silicon stations within a telescope much further apart (1 m providing a longer lever
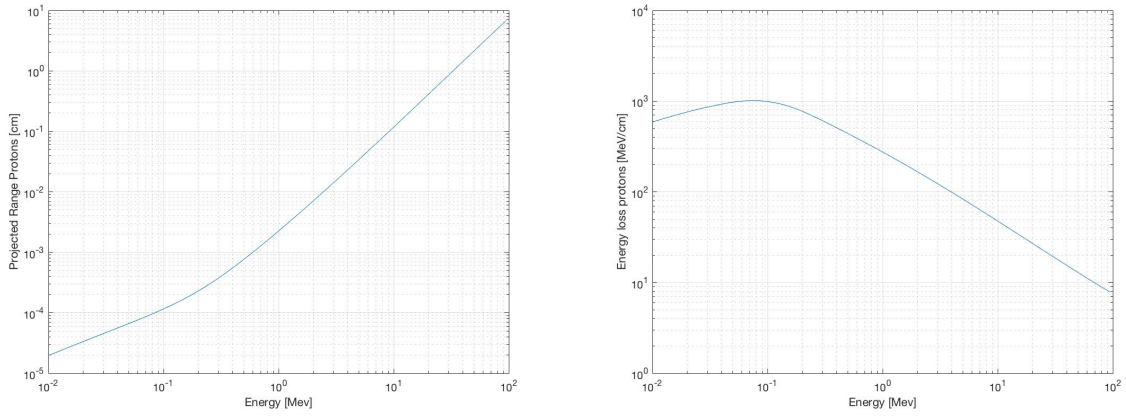
Figure 28: Projected range (left) and specific energy loss (right) for protons in scintillator for different kinetic energies [59].

arm. For the purpose of this proposal, we assume that we can improve on the angular resolution such as to achieve a resolution of $\Delta Q^2 = 1.4 \cdot 10^{-4}\,(\text{GeV}/c)^2$ by:

1. replacing the thick solid target with a pressurised gaseous hydrogen target
2. increase the spacing of silicon telescope to roughly match multiple scattering effects in the silicon itself and
3. run also with a lower beam energy of 50 GeV to reach the lowest values of Q^2. Muon scattering angles double going from 100 to 50 GeV beam energy.
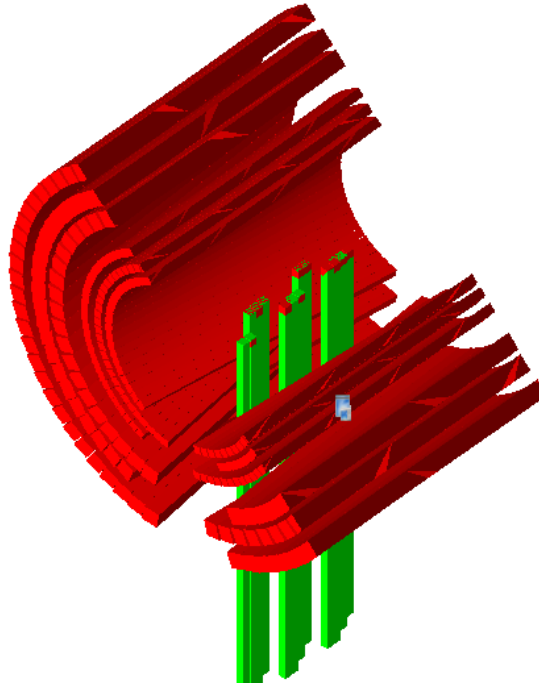
Figure 29: Layout of the active target made from scintillating fibres arranged along the beam direction.
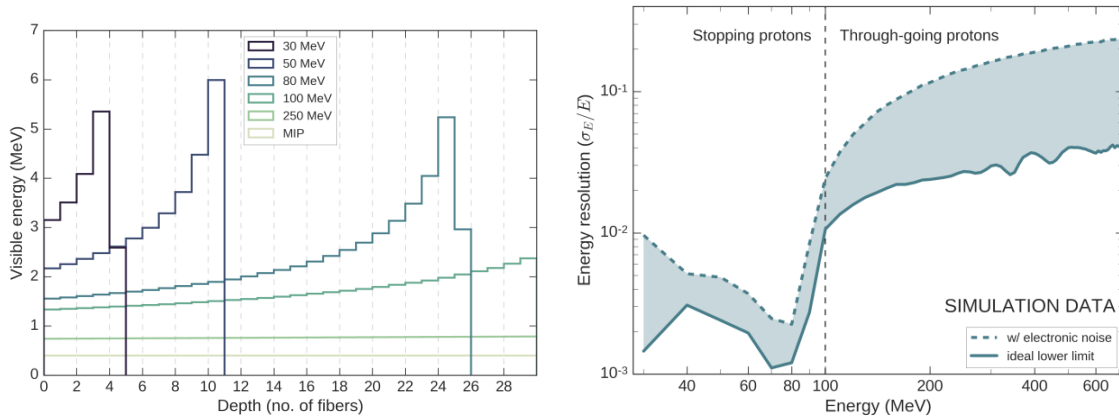
Figure 30: Left: Expected energy loss in individual fibres traversed by recoil protons for different proton energies. Right: energy resolution obtained by Bragg-curve fitting using simulation data. Work in progress and data are still very preliminary

2.5 Beam and count rates

We assume the standard COMPASS muon beam at a nominal beam energy of 100 GeV. The beam has the following parameters:

In order to calculate the integrated luminosity for this experiment we make use of the parameters outlined in Table 2. Assuming a 60 cm long gaseous hydrogen target operated at 4 bar pressure we obtain an integrated luminositiy for 80 days of running of $L = 8.9 \cdot 10^5 \, \text{mb}^{-1}$.

2.6 Trigger

One of the challenges of this experiment is the trigger. Reaching down to low values of Q^2 requires to trigger on signals of low-energy recoil protons. Assuming the TPC to be divided longitudinally into individual cells of length 10cm leads to a constant background noise from beam and halo muons of 20 keV per traversing particle. The drift time of electrons in hydrogen at 4 bar is about $2\,\mu\text{s/cm}$, thus $20\,\mu\text{s}$ for 10 cm. We may consider two scenarios, one using the full beam intensity and the other one a much reduced intensity, both scenarios being connected to a particular trigger scheme.

- Assuming an instantaneous beam rate of $4 \cdot 10^7 \mu/s$ we expect a continuous ionisation signal of about 80 keV within this time window. Therefore, a threshold of about 240 keV must be set ($3\sigma$) for triggering. With a mean energy for ion production in hydrogen of about 30 eV [60] this corresponds to about roughly 7,500 electrons, which is far above the electronic noise of a possible readout preamplifier[4]. The common drawback for all such trigger schemes is the long trigger latency of more than $20\,\mu\text{s}$ owing to the long drift time (see Section 2.14). Owing to the thin target, this does not pose a problem for elastic scattering events for trigger thresholds above a few $10^{-5}\,(\text{GeV}/c)^2$ as elastic event rates are below $10^4/s$. However, the present COMPASS readout does not allow for a trigger latency above about $2\,\mu\text{s}$ ($4\,\mu\text{s}$ if we half the clock frequency for the readout via APV). This is far below any reasonable drift time in a TPC, unless we reduce the gap-size (drift length) to less than 1 cm.

[4] we may assume the standard COMPASS APV readout for offline analysis which shows a noise of 1,500-2,000 electrons for GEM and silicon detectors, but cannot be used for triggering

Table 2: COMPASS μ-beam parameters and typical numbers used to estimate total count rates and accuracies. We assume an maximum trigger rate of 100 kHz. We also apply scaling by a factor 14 to convert the maximum beam intensity to a time averaged intensity including duty cycles, SPS and COMPASS efficiencies, as derived from experience. Numbers denoted by (*) are used to derive the integrated luminosities.

beam energy	100 GeV
muons per spill (max)	$2.7 \cdot 10^8 \, \mu/\text{spill}$
spill length	4.8 s
mean duty cycle	18%
spills per minute	3.3
efficiency of SPS	0.8
DAQ, veto dead times*	0.5
instantaneous intensity μ/s (scifi trigger)	$5 \cdot 10^7 \, \mu/\text{s}$
effective maximum beam rate	$4 \cdot 10^6 \, \mu/\text{s}$
mean effective intensity* μ/min (scifi trigger)	$2.4 \cdot 10^8 \, \mu/\text{min}$
instantaneous intensity μ/s (beam trigger)	$2 \cdot 10^5 \, \mu/\text{s}$
mean effective intensity* μ/min (beam trigger)	$1.2 \cdot 10^6 \, \mu/\text{min}$
beam spot size	$8 \times 8 \text{ mm}^2$
beam divergence	1 mrad
total days of beam time*	180
beam time for each pressure setting*	80
beam time for SciFi target*	20
target length H_2 target*	60 cm
target length SciFi* $(CH)_n$	1 cm
integrated luminosity H_2 @ 4bar	$8.9 \cdot 10^5/\text{mb}$
integrated luminosity H_2 @ 20bar	$4.45 \cdot 10^6/\text{mb}$
integrated luminosity SciFi target (hydrogen part only)	$3.33 \cdot 10^8/\text{mb}$

– As count rates are not an issue for very low values of Q^2, we might envisage to reduce the beam intensity by a factor 25 for dedicated data takings allowing to strongly reduce pile up. We would use a "simple" beam trigger and assume the veto system to define the beam and the surrounding target to cut the intensity by a factor of two (to be confirmed by a dedicated simulation). As event sizes are very small, we may run with trigger rates of about 100 kHz. This would require a beam rate of $2 \cdot 10^5 \mu/\text{s}$. For larger values of Q^2, an active scintillator target could be used.

– For high values of Q^2 ($> 3 \cdot 10^{-2} \, (\text{GeV}/c)^2$) corresponding to kinetic energies for recoil protons above 15 MeV and proton ranges above 2.5 mm) we will rely on a trigger from the active target, which can simply be obtained by a cut on the total energy observed in combination with a minimum number of scintillating fibres with signals above threshold. Such a system is presently being designed for space application of such a detector, operating in a self-triggering mode.

2.7   Normalisation

The key requirement for this experiment is an excellent point-to-point normalisation accuracy of below 0.1%. Unlike previous experiments at electron beam accelerators with precision magnetic spectrometers having low solid angles, the COMPASS spectrometer has full acceptance over the entire Q^2 range. Thus, in principle we can determine the differential cross section without normalising different subsets of measurements. However, this seems impractical as we need to modify the target system/target pressure in order to access the different regions of Q^2 with high individual statistical accuracy. We thus foresee the experiment to be done using two different types of targets and, using the TPC target, to take data with 2–3 different values for the target pressure (see discussion in Section 2.9). Owing to the short range of recoil protons with energies below 1 MeV we envisage performing a very low Q^2 run at a pressure of 1 bar. As the count rates are very high, this run can be performed within a few days. In order to cover the range of about $10^{-3} < Q^2 < 3 \cdot 10^{-2} \, (\mathrm{GeV}/c)^2$ we need two long data taking periods at 4 bar and 20 bar. A precise measurement of the beam intensity and the control of target pressure and temperature should give the corresponding luminosities with very high precision. However, in order to guarantee good matching, we can perform pressure scans. As the pressure scans will be used to calibrate the count rates in the effective overlap regions, the normalising runs can be kept short. A normalising region is defined by the largest values of Q^2 for one pressure regime, for which statistical errors are below 1%. As the count rates for the next pressure setting are much larger, sufficient statistical accuracy can be obtained quickly[5].

Although form factors and thus the proton radius can be extracted from the functional form of the acceptance-corrected Q^2-dependent count rates, absolute normalisation of the differential cross section serves as an additional measure of comfort. For this, the luminosity and absolute efficiencies have to be determined. The luminosity determination requires beam flux measurements and determination of the fiducial target thickness. The latter can be controlled up to very high precision as outlined in Section 2.13. For the beam flux, COMPASS features a method for a precise flux determination using a random trigger, which takes automatically into account DAQ dead time and beam reconstruction efficiencies. Possible effects from VETO dead times will have to be studied for the concrete trigger layout and a controlled way for correction is to be developed.

Last but not least we need a high accuracy for the full reconstruction efficiency.

2.8   Calibration

Calibration of the absolute Q^2-scale is a key element. As Q^2 can be measured by both muon scattering-angle and proton recoil-energy, we can cross check the relative calibration. The resolution of the scattering angle is solely determined by geometry, position resolution of the silicon detectors, multiple scattering in the target and alignment of the detectors. The latter one can be achieved using through-going muons. We may also cross check luminosity and resolutions using $\mu - e$ scattering occurring as background process. However, electrons will be forward going and thus require a dedicated trigger built from ECAL 2. Such a trigger system has already been set-up and operated for Primakoff measurements at COMPASS. The analysis of $\mu - e$ scattering is even more challenging than $\mu - p$ owing to Bremsstrahlung of electrons all along the spectrometer.

---

[5] depending on the stability of the system and the quality of the luminosity matching, we might even envisage to slowly scan the region of $10^{-4} < Q^2 < 3 \cdot 10^{-2} \, (\mathrm{GeV}/c)^2$ by slowly stepping up the pressure, thereby optimising beam time.

2.9 Estimates of the statistical uncertainties

Without accounting for trigger and reconstruction inefficiencies we can calculate the precision achievable within COMPASS using the boundary conditions outlined in Table 2.

We assume a triple experiment, one using a hydrogen TPC and a beam trigger at an instantaneous beam rate of $2 \cdot 10^5 \mu/s$ with two different target pressures, and third a scintillating fibre target of $1\,\mathrm{cm}$ length and an instantaneous beam rate of $5 \cdot 10^7 \mu/s$. We assume a transition in Q^2 between the different target coverages around $Q^2 = 0.3\,(\mathrm{GeV}/c)^2$. The cross-section behaviour is shown in Fig. 31a. The ratio of count rates expected for two scenarios for $\sqrt{\langle r_e^2 \rangle} = 0.84$ fm and $\sqrt{\langle r_e^2 \rangle} = 0.88$ fm is shown in Fig. 31b. We assume 100 bins equally spaced in $\log(Q^2)$ within the range of $10^{-4} < Q^2 < 1\,(\mathrm{GeV}/c)^2$. Statistical errors for each bin stay well below 1%.
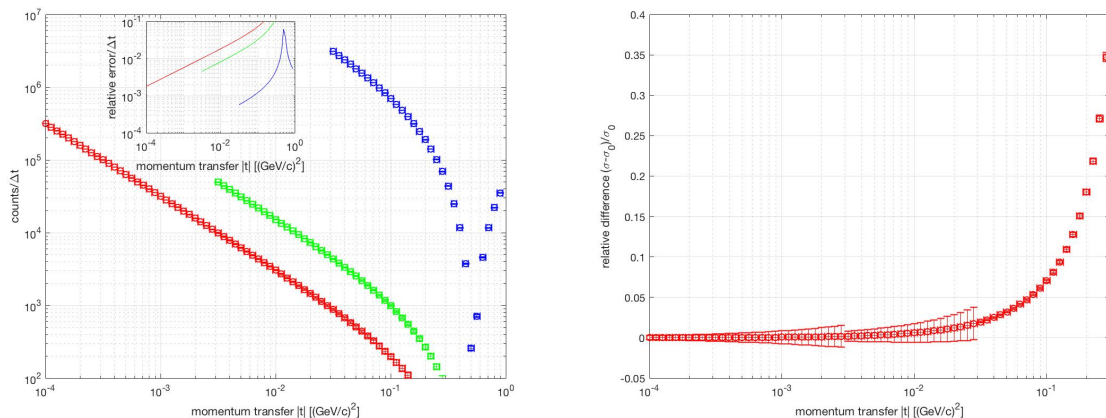
Figure 31: Left: Differential count rate dN/dt for elastic scattering events. The inset shows the relative statistical uncertainties expected. Right: Ratio of two possible scenarios for $\sqrt{\langle r_e^2 \rangle} = 0.84$ fm and $\sqrt{\langle r_e^2 \rangle} = 0.88$ fm (the latter is denoted as σ_0). We assume a triple measurement with three targets.

2.10 Radiative corrections

We have calculated radiative corrections to the elastic scattering process. The calculations are based on [61] with corrected mass values for the proton, which is considered to be structureless. In terms of the radiative corrections, which are relative to the leading scattering process, this is considered to be a sufficient approximation, despite further structure effects should be looked at more closely. They are given in the usual manner, as a correction term δ which connects the one-photon exchange cross-section and the higher-order (measured) process by $d\sigma = d\sigma_{1\gamma}(1 + \delta)$. The corrections include vertex corrections, loop corrections and two-photon exchange as shown in Fig. 32. The loop correction also include low mass pion loops (without ρ contributions). The results are displayed in Fig. 33a and show these corrections to be of order 1% at low values of Q^2 and (-1)–(-3)% at large values. Thus, these corrections are small compared to the case of electron scattering, as performed at low energy accelerators depicted in Fig. 33b) for comparison. The results show a logarithmic and thus weak dependence on the effective soft photon cut-off and which can only be determined through detailed simulations and is assumed to be 50 MeV for these calculations (10 MeV for the electron case).

Uwdligure c. Tree diagrams

Uwdligure d. One-loop diagrams

Uwdligure'è.'One-photon'loop'diagrams

Figure 32: Diagrams contributing to radiative corrections in the μp elastic scattering process. The proton is assumed to be structureless. Figure taken from [61].

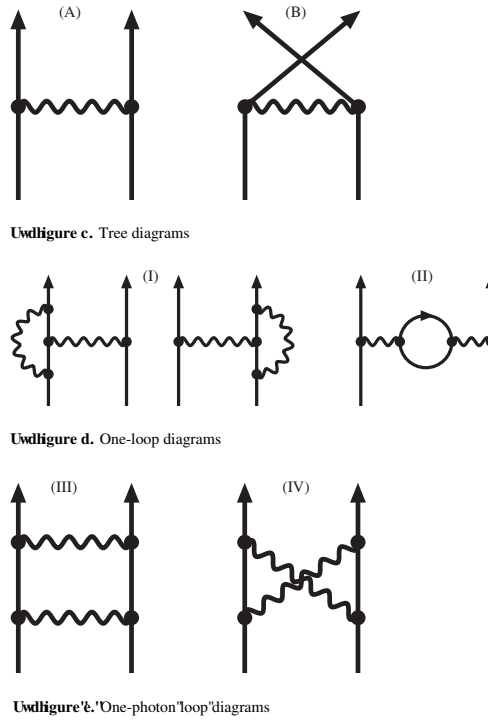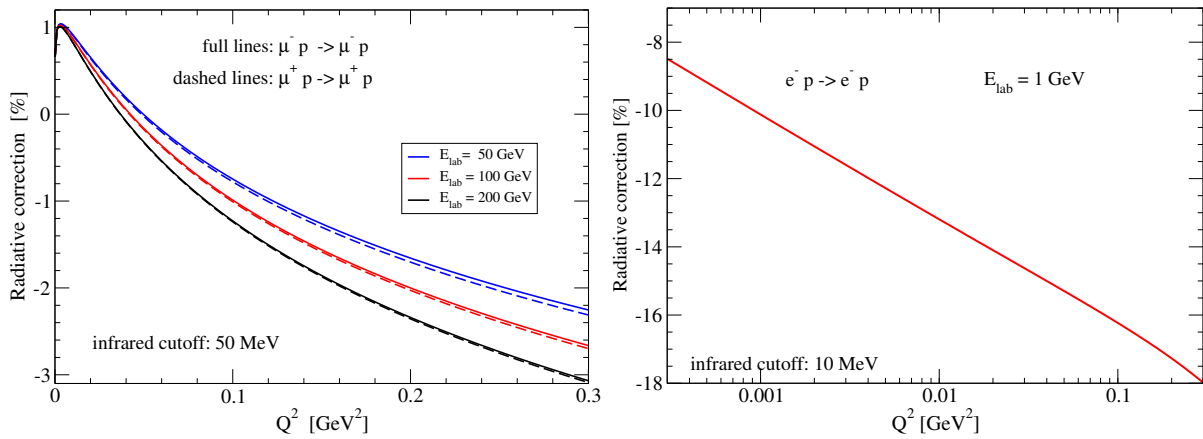Figure 33: Radiative corrections calculated according to Fig. 32. Left: μ^-p for three different values of $E_{\text{beam}} = 50, 100, 200$ GeV, right: e^-p with $E_{\text{beam}} = 1$ GeV.

2.11 Systematic uncertainties
2.11.1 Magnetic form-factor effects
For extracting the electric form factor and the charge radius, we need to correct for the magnetic contribution to the cross-section, which grows quickly for $Q^2 > 0.03\,(\mathrm{GeV}/c)^2$. Within our assumption on the form-factor parametrisation, the influence of the magnetic form-factor grows from 6% at $Q^2 = 0.03\,(\mathrm{GeV}/c)^2$ to as large as 60% at our largest values of $Q^2 = 0.3\,(\mathrm{GeV}/c)^2$, cf. Fig. 34 . The magnetic form-factor is known to better than 1% at larger Q^2 where its contribution matters, so the relative uncertainty from the magnetic correction ranges from 0.06% to about 0.6% for the cross sections for the large Q^2 setting. This has to be compared with the size of the effect to be measured, namely the sensitivity of the cross-section to the value of the proton radius, being 2% and 30%, respectively. Thus, the uncertainties are small as compared to the required precision.
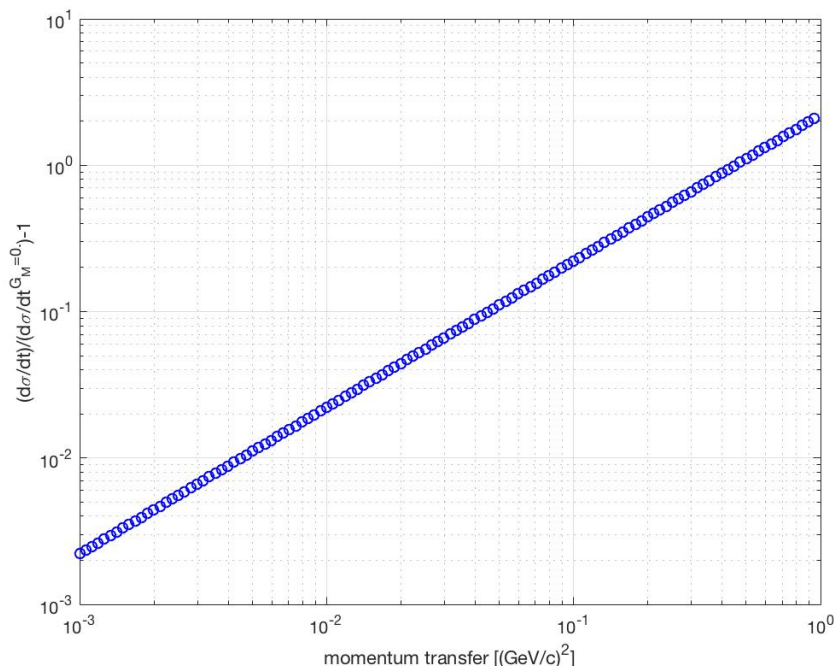
Figure 34: Relative contribution of the magnetic form factor to the elastic cross-section for different values of Q^2. The cross-sections are evaluated using Eq. (2) with $E_{\mathrm{beam}} = 100\,\mathrm{GeV}$.

2.11.2 Variation of beam charge and energy
The COMPASS beam environment allows for a wide range of systematic studies and we seem to only be limited by the available beam time.

- Ever since the discrepancy in the proton form factors obtained from the Rosenbluth separation and polarisation measurements, the reliability of the estimate for the two-photon exchange contribution has been questioned. The two-photon exchange is responsible for the Coulomb cross-section being different for equal and opposite charged particle interaction. However, the Olympus collaboration has performed a dedicated experiment comparing electrons and positrons in the last particle physics experiment performed at DESY. They determined the hard

two-photon exchange contributions and concluded that the resulting values for the ratio of e^-p to e^+p ($R2\gamma$) are smaller than some hadronic two-photon exchange calculations predict, but are in reasonable agreement with a subtracted dispersion model and a phenomenological fit to the form-factor data [62]. These investigations covered a wide range of virtual photon polarization of $0.456 < \epsilon < 0.978$. Still, the issue has been brought up again in the context of the proton radius puzzle and MUSE has planned for a dedicated measurement.

– As outlined in Section 2.1, lepton universality arguments have been put forward to explain the proton radius puzzle. The arguments for this rather exotic effect have weakened drastically with the redetermination of the Rydberg constant and the subsequent reevaluation of the proton radius from Lamb-shift measurements in electronic hydrogen. Nevertheless, an issue remains in what concerns radiative corrections, which are much smaller for muon induced than for electron induced reaction (see also Section 2.10). COMPASS can perform in situ measurements with high energy secondary electrons (positrons) produced in T6 and transported through the M2 beam line. Initial calculations by EN-EA show no principle limit from production for which estimated beams of up to 10^8 electrons could be derived. The main limitation will be given due to radiation protection restrictions in EHN2 and thus through the purity of the beam. In order to guarantee an efficient transmission of the electron beam, the quality of vacuum in M2 needs to be improved, mainly through scrapers and beam instrumentation. With a conservative estimate of a beam with an intensity of $10^6\,e^-/s$, we would be able to repeat the measurements for a small region of low Q^2 (e.g. $Q^2 < 5 \cdot 10^{-3}\,(\mathrm{GeV}/c)^2$) within a shorter beam time.

– The relative accuracy for the determination of Q^2 using the scattered muon depends weakly on Q^2, as muon scattering angles in the laboratory system grow towards lower beam energies (Fig. 15). Also radiative corrections depend on the energy of the incoming beam (Fig. 33a). However, for the latter only large values of Q^2 are sensitive to the beam energy and thus a systematic study seems beam time consuming.

2.11.3 Variation of target material

The proposed set-up using a high-pressure target TPC allows for a rapid change of target material. We can easily exchange hydrogen with deuterium or helium and thus perform a precision measurement of these radii as well. The mean square charge radius of deuterium has recently been determined using muonic deuterium [63] and further measurements with other elements are planned by the CREMA collaboration [64, 65]. If the proton radius puzzle still persists, it would be highly desirable to also investigate other charge radii using muon scattering techniques. Using CH_2 we may also address the carbon charge radius. Discrimination against quasi-elastic scattering events has still to be carefully investigated.

2.12 Further developments

The present proposal has assumed a rather conservative data taking, which relies on a simple beam trigger and a simple Scifi multiplicity trigger. However, the beam trigger leads to a rather inefficient use of beam time as the beam intensity has to be reduced by a factor 100 as compared to the maximum. This in particular affects the high-Q^2 data points for each individual target setting, which in turn determines the beam time required. Two scenarios could in principle be envisaged:

Figure 35: CAD study of the COMPASS TPC (Gatchina group) in different views.

– Recoil proton trigger: Triggering on recoil protons using the TPC is difficult owing to the long drift time and the comparatively low latency allowed by the existing COMPASS DAQ. The system being developed by the Gatchina group for their experiment at Mainz cannot be used easily. Thus, we would need a signal based on scintillation light (either from hydrogen or from scintillating fibres surrounding the hydrogen target). No scheme of this type has yet been developed.

– Scattered muon trigger: The challenge is to detect a small scattering angle of the muon in real time with a maximal latency of 0.5μs. At present, all micro pattern detectors are equipped with the APV readout chip, which has a pipelined architecture and requires a readout time of 0.5μs. For the four silicon stations, such a system would have to be replaced in favour of a parallelised system, which feeds its data into a FPGA array. The track reconstruction algorithm is then required to single out noise and to reconstruct the relative angle of incoming and outgoing beam particle track. As such a trigger would only be necessary for $Q^2 > 10^{-3}\,(\text{GeV}/c)^2$, where the scattering angle exceeds $300\,\mu$rad, an alignment on the hourly basis is not required.

2.13 Details on the TPC

The design of the TPC is motivated by the exact knowledge of the fiducial volume for reconstructable elastic scattering events. This requires high precision on the gas density and geometrical parameters, the exact characterisation of the active TPC volume.

Driftspace: in order to shape the drift field, twenty field correction rings are placed in the outer TPC region between the cathode and the grid to form the uniform electric field in the drift space. The high voltage distribution includes -100 kV on the Cathode, -7 kV on the grid, 0 kV on the anode at 20 bar pressure. The HV is distributed for the field compensating rings with a resistor divider. The HV will be known with 0.01% absolute precision.

H_2 gas purity: in order to avoid the losses of the ionisation electrons during the drift time, the contamination of the H_2 gas by any electro-negative gas (O_2, H_2O) should be reduced to a level below 1 ppm. This will be achieved by continuous H_2 purification with a special gas purification system, similar to that described in [66], which eliminates gas impurities down to smaller than 0.1 ppm.

Number density: the number N of protons per cm^3 in hydrogen gas depends on the pressure p_{tech} and temperature T_0. We will control the pressure to 0.01% absolute precision and keep the temperature constant to a level ± 0.050 (0.014% absolute precision). This determines the proton density with 0.025% absolute precision, as planned by the Gatchina group.

Time, recoil energy, and recoil angle resolution: the anode channels will be equipped with low noise preamplifiers with the noise at the level of 20 keV (σ). Such numbers can be achieved using a custom made preamp (Gatchina) or by the SAMPA ASICs developed for the ALICE TPC upgrade (ENC: 680 e^- noise).- This determines the recoil energy resolution. Depending on the range of the recoil proton, the recoil energy is obtained by the sum of energies deposited against the anode pixels. Accordingly, the noise will be summed up as well. So the energy resolution for maximal proton range ($T_{rec} \sim 10$ MeV for 20 bar, $T_{rec} \sim 4$ MeV for 4 bar) will be around $\sigma_E \sim 60$ keV. Note, however, that the noise might be larger in the presence of the muon beam and strongly depends on the segmentation of the anode plane.

The expected signal arrival time resolution is[6] $\sigma_t = 40$ ns. The angular resolution σ_{θ_R} is limited by Coulomb scattering of the recoil protons with $\sigma_{\theta_R} \sim 10$ mrad. θ_R is measured by the differences in arrival times of the signals from the anode pixels crossed by the recoil. The precision of such measurements varies from $\sim \pm 10$ mrad (signals from two neighbouring pixels) to $\sim \pm 2$ mrad for long ranged protons. So the final recoil angle resolution will be from 15 mrad to 10 mrad (for proton range $60 - 80$ mm and ~ 300 mm, respectively).

Electron drift velocity and track diffusion in TPC: The electron drift velocity is $v_1 \approx$ 0.42 cm/μs in the TPC drift region and $v_1 \approx 0.75$ cm/μs in the region of the anode grid. The value of v_1 should be known with high precision (better than 0.1%) as it determines

---

[6] at present, we do not have the time resolution for the option of the SAMPA ASICs

the fiducial gas target thickness (important for an absolute cross section measurement) and determines the coordinate of the interaction point along the beam direction.

Gas target length: the gas target length, L_{tag}, is determined from the measured difference between maximal and minimal arrival times of the TPC signals in the chosen drift space, $L_{tag} = (t_{arr}^{max} - t_{arr}^{min}) \cdot v_1$. Only a small correction to t_{arr}^{max} might be needed for track diffusion. The expected precision in L_{tag} determination is 0.02% for $L_{tag} = 20$ cm.

Vertex z coordinate - calibration and resolution: calibration of the scale of the coordinate z along the beam direction will be done simultaneously with measurements of the drift velocity at the electron beam at MAMI. For this, the TPC setup will be slightly turned so that the electron beam (in position $z = 10$ mm) will cross the HV plane in the TPC central region thus producing ionisation at z close to $z = 0$. Registration of these signals can fix the z scale in TPC with absolute precision better than 100 μm. Care has to be taken to account for the difference in electronic delays between the beam trigger and TPC signals at the calibration and main experiments. Another way to determine $z = 0$ can be the in situ detection of the beam muon signals on the central anode in the nominal zero degree TPC position. The $z = 0$ point can be found by analysing the trailing edge of these $\sim$ 100 μs long signals. Advantage: such measurements can be done at any time in the course of the main experiment (with beam intensity reduced to 10^3 μ/s). The main disadvantage is relatively large systematic uncertainty determining the $z = 0$ point. The optimal solution would be calibration of this method again by the 90°setup measurements. Then it can be used as a stability control for the z scale calibration in the course of the experiment. As to the longitudinal z resolution in detection of the recoil protons, it depends on the arrival time resolution. The z-resolution is expected to be $\sigma_z \sim 200$ μm.

2.14 Drift in gaseous hydrogen

For exercise we shall assume a total drift path in the TPC of 10 cm with a field applied of $E = 10$ kV resulting in an electric field strength of 1 kV/cm. At a pressure of 4 bar, the number density of hydrogen atoms is about $2.14 \cdot 10^{21}$ cm^{-3} and thus E/N becomes $5 \cdot 10^{-19}$ V·cm^2 or $5 \cdot 10^{-2}$ Td. According to Fig. 36, the drift velocity for electrons is $v_e = 1$ mm/μs and hydrogen ions travel with roughly 10^{-4} cm/μs. Thus, the maximal drift time for electrons becomes 100μs and ions build up over $\tau_{H^+} = 0.1$ s. Assuming an instantaneous beam intensity of $I_\mu = 4 \cdot 10^7 \mu$/s and an energy loss of $E_{loss} = 20$ keV, with $W_I = 30$ eV per ion pair produced, we obtain:

$$N_{H^+} = I_\mu \cdot \frac{E_{loss}}{W_I} \cdot \tau_{H^+} = 0.88 \cdot 10^9 \tag{5}$$

hydrogen ions in the drift volume over the time of a spill.

2.15 New Collaborators

The proposal extends the physics scope of COMPASS and thus would allow to attract new collaborating groups: The group of PNPI Gatchina, experienced in active high pressure hydrogen targets has expressed strong interest to join COMPASS for this measurement. This group has performed radius measurement at GSI [57], contributed with a high pressure hydrogen TPC for the MUCAP experiment at PSI [68, 69] and plans for further employment of their technology at FAIR. They are also key players for the new letter of intent using this technology at MAMI.
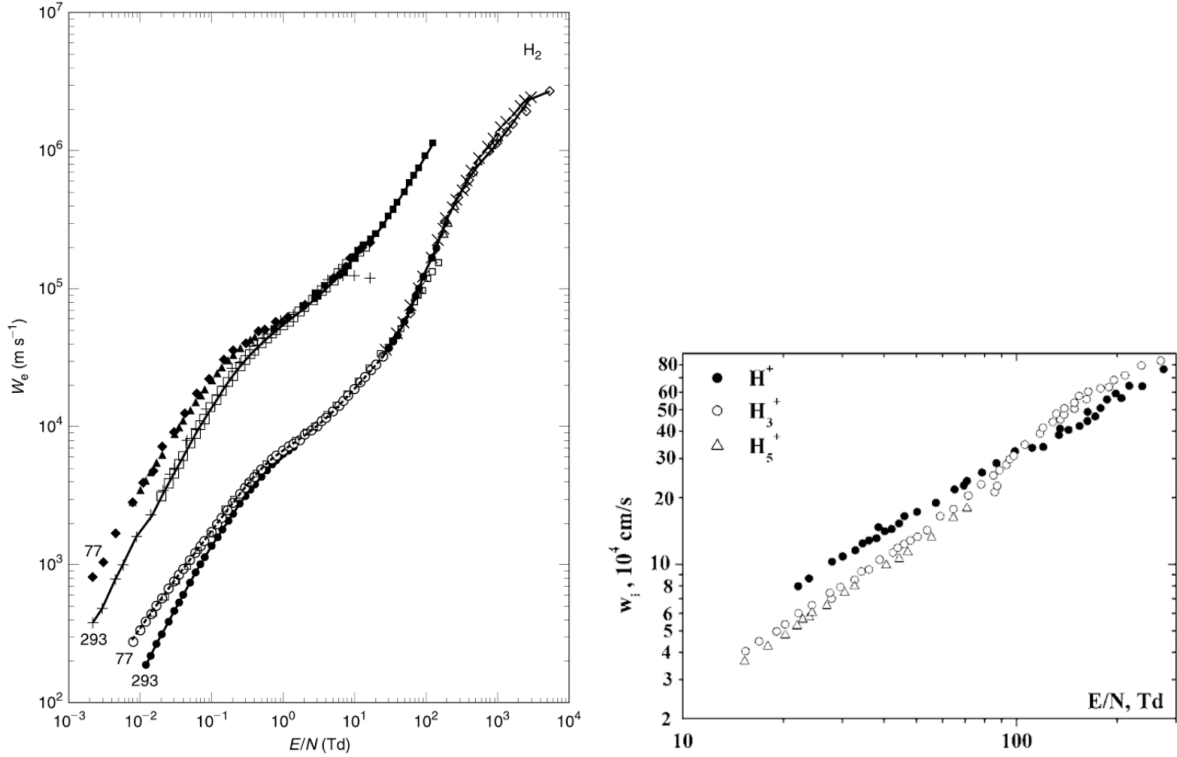
Figure 36: Drift velocities for electrons and protons in hydrogen and deuterium (scaled by a factor 10) [67]. Note that $E/N = 1$ Td corresponds to 10^{-17} V·cm^2 and $N = 5.4 \cdot 10^{20}$ cm^{-3} at 1 atm.

2.16 Precision and Impact of the COMPASS measurement

A preliminary Monte Carlo study of the proposed set-up employing the high-pressure hydrogen TPC has demonstrated [70] that the achievable precision on the proton radius is better than 0.01 fm, thus capable of distinuishing the debated values $\langle r_{ep}^2 \rangle =$ 0.84 and 0.88 fm.

Given the currrent experimental efforts undertaken for this fundamental quantity as descibed above, it seems timely to take data at COMPASS in 2022. For a successful running in 2022 with the TPC as an essential new component, it will be important to foresee first test measurements, best in the beginning of the 2021 beam time.

Independent of the progress that the analyses of planned and ongoing electron scattering experiments (MAMI, JLab), the low-energy muon scattering experiment MUSE (PSI) and further data from atomic spectroscopy will make, the approach by high-energy elastic muon scattering off the proton remains unique, in terms of determining the proton form factor behaviour in the low- to medium-Q^2 region. Due to the lower systematic effects *e.g.* regarding the radiative corrections, this measurement poses in any case a decisive test of the results obtained by electron scattering since many decades.

– HARDWARE UPGRADES –

3   Experimental requirements for the transverse deuteron run

The set-up for the transverse deuteron run is similar to the running conditions of the previous years, so the main issue is to preserve the readiness of the detectors, and especially the polarised target, for 2021.

4   Experimental requirements for the proton radius measurement

The apparatus requirements imposed by this new measurement are rather modest, but do require additional detectors. These concern the target TPC and the SciFi active target recoil detector. As the determination of the muon scattering is vital, we have to refurbish at least one silicon station. In addition, we need longer optical benches to achieve internal stability for both silicon telescopes and minimise thermal displacements. Although the beam is very pure with a pion contamination below 10^{-5} we should adapt the existing muon filter at the downstream end of the COMPASS experiment for the elastic scattering kinematics. The installation of new detectors also imposes requirements on new electronics and their implementation into the COMPASS DAQ scheme.

Detector	Responsibility	needed [y/n]	new/existing
μ Beam	CERN	y	existing
electron Beam	CERN	y ?	new
BMS		y	existing
Luminosity measurement		y	new
Silicon telescopes	TUM	y	existing
Silicon station	TUM +++	y	new
TPC and pressure tank	Gatchina	y	new
TPC gas system	Gatchina	y	new
TPC RO	Gatchina, Bonn HISKP, Freiburg, Saclay ++	y	new
SciFi target	TUM++	y	new
SciFi tracker		y	existing
GEM	Bonn HISKP ++	y	refurbished
Micromega	Saclay ? ++	y	existing
Straws	-	n	
MWPC	-	n ?	
DC	-	n ?	
RICH	-	n ?	
HCAL	-	n	
ECAL 0	-	n	
ECAL 1	-	y for e-beam	
ECAL 2	-	y for e-beam	
MW1	-	n	
MW2	-	n/y ?	
W45	-	n	
DAQ	TUM, Prague ++	y	
Trigger	Bonn PI, Mainz ++	y	
Slow control	Lisbon	y	
Online analysis		y	
Installation	CERN		

Table 3: **tentative and very preliminary** Requirements and responsibilities for equipment

Acknowledgements

The authors thank J. Bernhard, M. O. Distler, N. Kaiser, ... for useful advice and comments, critical reading, and/or technical help.

References

 [1] P. J. Mulders et al., Nucl. Phys. B461 (1996) 197, [Erratum: Nucl. Phys. B484, 538 (1997)] We use the "Amsterdam notation" as in this publication.

 [2] V. Barone et al., Prog. Part. Nucl. Phys. 65 (2010) 267.

 [3] C. A. Aidala et al., Rev. Mod. Phys. 85 (2013) 655.

 [4] H. Avakian et al., Eur. Phys. J. A52 (6) (2016) 150, [Erratum: Eur. Phys. J. A52 No.6 (2016) 165].

 [5] A. Kotzinian, Nucl. Phys. B441 (1995) 234.

 [6] A. Bacchetta et al., JHEP 02 (2007) 093.

 [7] COMPASS, Collaboration, Addendum 2 to the COMPASS Proposal, CERN-SPSC-2009-025 SPSC-M-769, SPSLC-P-297 Add.2 (2009).

 [8] D. W. Sivers, Phys. Rev. D41 (1990) 83.

 [9] J. C. Collins, Nucl. Phys. B396 (1993) 161.

[10] HERMES, A. Airapetian et al., Phys. Rev. Lett. 103 (2009) 152002.

[11] COMPASS, C. Adolph et al., Phys. Lett. B717 (2012) 383.

[12] COMPASS, C. Adolph et al., Phys. Lett. B717 (2012) 376.

[13] COMPASS, C. Adolph et al., Phys. Lett. B736 (2014) 124.

[14] Belle, K. Abe et al., Phys. Rev. Lett. 96 (2006) 232002.

[15] Belle, R. Seidl et al., Phys. Rev. D78 (2008) 032011, [Erratum: Phys. Rev. D86, (2012) 039905].

[16] M. Anselmino et al., Phys. Rev. D75 (2007) 054032.

[17] A. V. Efremov et al., Eur. Phys. J. ST 162 (2008) 1.

[18] COMPASS, E. S. Ageev et al., Nucl. Phys. B765 (2007) 31.

[19] Jefferson Lab Hall A, X. Qian et al., Phys. Rev. Lett. 107 (2011) 072003.

[20] Jefferson Lab Hall A, Y. X. Zhao et al., Phys. Rev. C90 (5) (2014) 055201.

[21] A. Martin et al., Phys. Rev. D91 (1) (2015) 014034.

[22] A. Martin et al., Phys. Rev. D95 (9) (2017) 094024.

[23] M. Anselmino et al., Phys. Rev. D87 (2013) 094019.

[24] M. Anselmino et al., Phys. Rev. D86 (2012) 014028.

[25] COMPASS, C. Adolph et al., Phys. Lett. B772 (2017) 854.

[26] J. Matouek, Few Body Syst. 58 (3) (2017) 126.

[27] M. Radici et al., JHEP 05 (2015) 123.

[28] COMPASS, C. Adolph et al., Phys. Lett. B753 (2016) 406.

[29] X. Artru et al., Z. Phys. C73 (1997) 527.

[30] X. Artru, Prob. Atomic Sci. Technol. 2012N1 (2012) 173.

[31] B. Parsamyan, Int. J. Mod. Phys. Conf. Ser. 40 (2016) 1660029.

[32] COMPASS, C. Adolph et al., Nucl. Phys. B865 (2012) 1.

[33] COMPASS, C. Adolph et al., Phys. Lett. B731 (2014) 19.

[34] J.-W. Chen et al., Nucl. Phys. B911 (2016) 246.

[35] T. Bhattacharya et al., Phys. Rev. D94 (5) (2016) 054508.

[36] A. Courtoy et al., Phys. Rev. Lett. 115 (2015) 162001.

[37] JLab, Hall-A Proposal E12-10-006, SIDIS with Transversely Polarized 3He Target using SoLID (2009), `http://hallaweb.jlab.org/collab/PAC/PAC35/PR-10-006-SoLID-Transversity.pdf`.

[38] JLab, Hall-A Proposal E12-11-108, SIDIS with Polarized Proton Target using SoLID (2011),
`https://www.jlab.org/exp_prog/proposals/11/PR12-11-108.pdf`.

[39] R. Hofstadter et al., Phys. Rev. 98 (1955) 217.

[40] CREMA, R. Pohl, Hyperfine Interact. 227 (1-3) (2014) 23.

[41] R. Pohl et al., Nature 466 (2010) 213.

[42] T. Suda, Electron scattering experiment off proton at ultra-low q^2 (2016),
`http://www2.yukawa.kyoto-u.ac.jp/~min2016/slides/Suda_MIN2016.pdf`,
`talkpresentedatMesoninNucleusconference`.

[43] R. J. Hill, EPJ Web Conf. 137 (2017) 01023.

[44] J. C. Bernauer, J. Phys. Conf. Ser. 381 (2012) 012006.

[45] A. Antognini et al., EPJ Web Conf. 113 (2016) 01006.

[46] PRad, A. H. Gasparian, JPS Conf. Proc. 13 (2017) 020052.

[47] M. Mihovilovi et al., Phys. Lett. B771 (2017) 194.

[48] J. J. Krauth et al., `arXiv:1706.00696`.

[49] R. Pohl et al., Metrologia 54 (2017) L1.

[50] J. C. Bernauer et al., Avoiding common pitfalls and misconceptions in extractions of the proton radius, in: ECT* Workshop on The Proton Radius Puzzle Trento, Italy, June 20-24, 2016, 2016.
`http://inspirehep.net/record/1468073/files/arXiv:1606.02159.pdf`

[51] P. Mergell et al., Nucl. Phys. A596 (1996) 367.

[52] I. T. Lorenz et al., Eur. Phys. J. A48 (2012) 151.

[53] MUSE, R. Gilman et al., `arXiv:1303.2160`.

[54] COMPASS, C. Adolph et al., Phys. Rev. Lett. 114 (2015) 062002.

[55] J. Bernhard, responsible for the M2 beam line at CERN, private communication (2017).

[56] N. Kaiser, TU Munich, private communication (2017).

[57] S. Ilieva et al., Nucl. Phys. A875 (2012) 8.

[58] A. A. Vorobyov et al., Nucl. Instrum. Meth. 119 (1974) 509.

[59] NIST, Values for stopping power and energy loss in hydrogen are taken from (2017), `https://www.nist.gov/pml/radiation-dosimetry-data`.

[60] B. E. Leonard et al., Radiation Research 55 (1973) 1.

[61] N. Kaiser, J. Phys. G37 (2010) 115005.

[62] OLYMPUS, B. S. Henderson et al., Phys. Rev. Lett. 118 (9) (2017) 092501.

[63] CREMA, R. Pohl et al., Science 353 (6300) (2016) 669.

[64] R. Pohl, Shrinking the proton, presentation at the PhiPsi2017 workshop at Mainz (2017).

[65] CREMA collaboration, F. Biraben et al., Proposal for an experiment at PSI: Lamb shift in muonic helium, `https://www.ethz.ch/content/dam/ethz/special-interest/phys/particle-physics/precisionphysicsatlowenergy-dam/Research/Proposal_muHe_pdf.pdf`.

[66] V. A. Ganzha et al., Nucl. Instrum. Meth. A578 (2007) 485.

[67] G. G. Raju.

[68] J. Egger et al., Eur. Phys. J. A50 (10) (2014) 163.

[69] S. M. Clayton, AIP Conf. Proc. 1222 (2010) 407.

[70] M. O. Distler, S. Uhl (U Mainz/TUM), private communication (2017).